Implementation of silicon nitride isolation trenches in SOI MEMS accelerometers

Bas van Laerhoven
master-thesis@basvanlaerhoven.nl
s1567381

***Abstract*—This paper presents the design of two capacitive SOI MEMS accelerometers. Both accelerometer designs use Silicon Nitride isolation trenches to create new methods for readout or actuation of the microchips. Both accelerometer designs maximise the available area of the microchip by using a readout structure suspended above the mass. The readout structure is realised in the device layer, the mass is located in the handle layer. One accelerometer design used EMAM to bring the readout structure to an oscillation. An extra modulation reduces the effects of outside parasitic sources. To test the accelerometers a measurement setup is designed and built, preliminary results show that the measurement setup functions as intended. The fabrication of the accelerometers could not be completed but the simulations show a functioning of the EMAM principle which reduces outside parasitic influences, and suppresses unwanted frequencies with a double demodulation. The expected sensitivity of both the chips is $3pf/\mu m$.**

***Index Terms* - MEMS, SOI, Accelerometer, Differential capacitive readout, Silicon Nitride trenches.**

I. Introduction

The design and fabrication of silicon on insulator (SOI) MEMS capacitive accelerometers is a constantly improving process. It all started with the mass-spring-damper system [1], it evolved to complex systems consisting of multiple parts that are able to pick up small vibrations with the highest sensitivity. Practically every accelerometer uses the principle of the mass-spring-damper system, but this can be used in numerous amounts of configurations and applications. For example in the method of readout, next to capacitive sensors there are resistive, piezoresistive, resonant or thermal accelerometer sensors [1].

Focusing on the category of capacitive accelerometers there are several ways how a readout can be realised. The distance between the plates can be variable, or the area of overlap can be variable. And also the placement and orientation of the capacitors can have a big impact on the outcome of the sensor [2], [3], [4]. When the type of sensor and method of readout are decided there are still various design choices left that effect the performance of an accelerometer. On of these choices is the design for the springs [5]. And an example of a complex structure that improves the functioning of accelerometers are anti-springs, which can create a very low or negative effective spring constants [6].

The goal of all these choices and innovations is to design an accelerometer that is perfectly fit for the necessary application. This can vary but generally it needs to be low cost, low power and have good dynamic characteristics. [7]

This paper presents the implementation of a new technology on SOI MEMS accelerometers. This technology involves using silicon nitride (SiN) isolation trenches. The use of SiN is not new to the semiconductor industry. In the production of integrated circuits SiN is often used as a barrier or insulator. Now this technology has found its way to the MEMS technology and with an updated fabrication process trenches of SiN can be created and used as an isolation layer.

In the MEMS technology, specifically for accelerometers, the SiN isolation trenches can be used in several occasions. With SOI wafers there is a separation between the device and handle layer, created by the buried oxide layer (BOX), but all devices in the device layer would always be connected to each other one way or the other. Figure 1 shows an illustration of a cross-section of a SOI wafer. The yellow silicon oxide (SiO_2) layer represents the BOX layer. Up until now structures were etched mainly in the device layer. The limitation of this is that the etched structures will always have a connection with other structures in the device layer or they will connect to the handle layer through the BOX layer. With the introduction of an isolating material there comes a new range of possibilities for designing accelerometers. In this research the use of this new technology is used in the design of two different accelerometers. Both accelerometers will use the SiN isolation trenches.

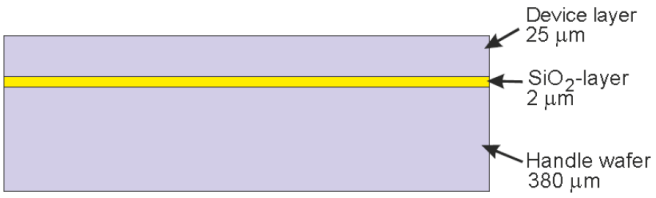

Fig. 1: Cross-section of an SOI wafer, showing the different layers.

The capacitive readout that will be used in the design of the accelerometers is realised by creating parallel plate capacitors

which change capacitance with a variable distance between the plates. Half of the parallel plates are fixed to the mass and the other half is fixed to a reference frame. Be applying an electrical signal to the reference frame charge will be transferred through the capacitor plates onto the mass. Using the mass as an output a movement results in changes in capacitance which can be measured. A simplified model of such a design is given in Figure 2. Where on the edges of the mass four springs are connected. In the middle there are four combs which consist of parallel capacitor plates. The top and the bottom combs are mirrored versions of each other to create a differential pair.

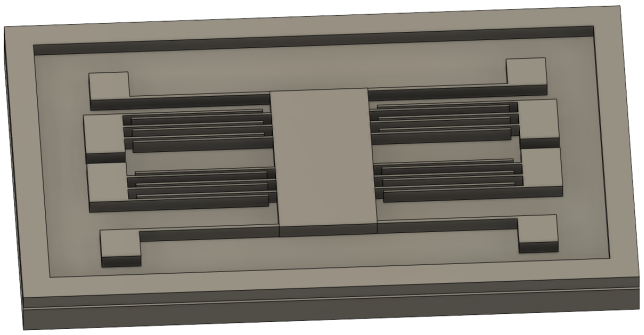

Fig. 2: 3D model of a simplified accelerometer design. The structures are created in the device layer.

This paper presents a new method for realising the readout of a capacitive accelerometer. The operating principle will be the same as discussed above and presented in Figure 2. The difference will be in the location of the readout which is made possible by using the silicon nitride isolation trenches.

The first accelerometer design uses the SiN trenches to create isolation between areas of the readout structure so that different capacitors are formed. By using this isolation the structure is mechanically connected and a bigger readout structure suspended above the mass can be designed. This uses the available area of the microchip more efficiently and leads to a higher sensitivity.

The second design introduces the principle of Electro Mechanical Amplitude Modulation [8] to the accelerometers. With the use of the SiN trenches actuators can be directly connected to the readout structure of the accelerometer. Because of the isolation the actuators can be operated without interfering with the readout. This enables the use of a double carrier of which it will be investigated if this is beneficial for interferences and noise suppression.

This paper will present the theory needed for the design of an accelerometer. Together with both the accelerometer designs and their unique features. The designs will be simulated to get an idea of the behaviour of the accelerometers. After the fabrication the accelerometer chips need to be tested so a measurement setup is designed, built and tested to prepare for the measurement of the microchips. Preliminary results of the measurement setup are discussed, as well as the performance of the designs in simulation.

II. Theory

A. Mechanical

MEMS accelerometers are based on the mass-spring-damper model, a model which is based on a mass that is connected with springs, and because of the small dimensions the air around the mass and springs acts as a damper. The equations of motion for a mass-spring-damper-model are derived with the sum of forces acting on the mass [9], which results in the differential equation given by equation 1. The working principle, with fundamental equations, is illustrated by Figure 3.

$$M\frac{d^2x}{dt^2} + D\frac{dx}{dt} + Kx = F_{ext} = Ma \tag{1}$$

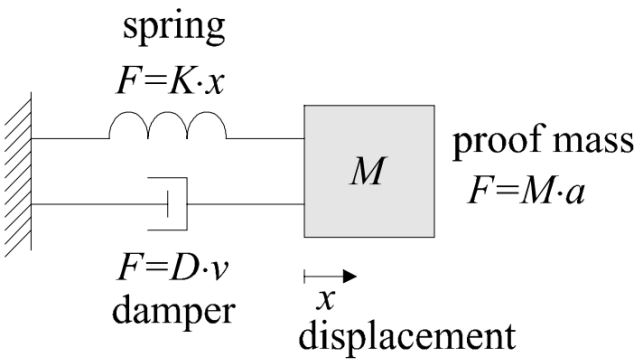

Fig. 3: Mass-spring-damper model used for an accelerometer [9].

The differential equation (equation 1) gives the dynamic behaviour of the model. D is the damping factor, K is the effective spring constant, M is the mass, F_{ext} is the external force which acts on the reference frame of the accelerometer. From this differential equation expressions for the resonance frequency (ω_r) and quality factor (Q) can be derived:

$$\omega_r = \sqrt{\frac{K}{M}} \qquad Q = \frac{\omega_r M}{D} \tag{2}$$

The resonance frequency is determined by the spring constant and the mass. When combining Hooke's Law and Newton's second law of motion the displacement can be expressed as:

$$x = \frac{F}{K} = \frac{Ma}{K} = \frac{a}{\omega_r^2} \tag{3}$$

The displacement of the mass is equal to the deformation of the springs and eventually to the movement of the parallel plate capacitors. Equations 2 and 3 show that there is a trade-off between the bandwidth and the sensitivity of an accelerometer.

B. Springs

Springs used for accelerometers vary from basic rectangular beams to pre-loaded and circular beams. But every complicated structure can be broken down to parts that always lead back to the same theory. When a structure is subjected to a load it will deflect, the direction and magnitude of this deflection is dependent on the properties of the structure. This is described with the spring constant (K). In Figure 3 it is visible that the spring constant is used in Hooke's Law to describe the force acting on the mass. The accelerometers presented in this paper use springs that can always be broken down to rectangular beams that are clamped at both sides (substrate and mass). Using the beam deflection theory we get an expression for the spring constant of a clamped-clamped rectangular beam [10] [11]:

$$K = \frac{Ehw^3}{L^3} \tag{4}$$

Where E is the Young's modulus, of in this case silicon, h is the height, w is the width and L is the length. In the design process the height will be fixed because it is determined by the height of the device layer.

When multiple springs are used, or springs are combined to make more complicated designs it is possible to calculate a spring constant for the entire structure, also called the effective spring constant (K_{eff}). In this case springs can either be placed in series or in parallel to each other.

$$Series : \frac{1}{K_{eff}} = \frac{1}{K_1} + \frac{1}{K_2} + ... + \frac{1}{K_n} \tag{5}$$

$$Parallel : K_{eff} = K_1 + K_2 + ... + K_n \tag{6}$$

C. Readout

In a capacitive MEMS accelerometer the displacement is measured by changes in capacitance. This is realised by connecting 'fingers' to the mass and the reference frame. Each set of 'fingers' form a parallel plate capacitor. When the parallel plate capacitors are placed next to each other they are often referred to as combs. One of the combs is connected to the mass and is free to move, the other comb is fixed to the reference frame. This principle is explained in Figure 4.

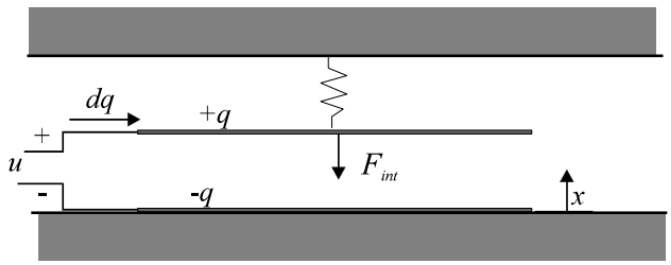

Fig. 4: Parallel plate capacitor with a fixed plate and a moveable plate suspended by a spring. An applied force results in a change in plate distance [12].

Since the plates can only move in one direction the capacitance can be expressed by:

$$C = \frac{\epsilon A}{x} \tag{7}$$

Where A is the overlapping area of the parallel plates, ϵ is the dielectric constant of air, and x is the distance between the parallel capacitor plates. A charge on the plates will cause them to move together, without a spring the increasing charge will keep moving the plates until they touch. With a spring there is an opposing force that can keep the plates stable and prevent them from collapsing onto each other. Typically if we move the parallel plate and after that remove the charge the spring will make the plate moves back to its original position. In a situation where no external force is applied the equilibrium position (x_{eq}) is given by [12]:

$$x_{eq}^3 - x_0 x_{eq}^2 + \frac{u^2 \epsilon A}{2K} = 0 \tag{8}$$

Where x_0 is the initial position of the parallel plate, u is the applied voltage and K is the effective spring constant. Generally this configuration remains stable as long as the equilibrium position is less than 2/3 of the initial position. beyond this point the parallel plate will collapse onto each other. The voltage at which this occurs is given by equation 9 [12]. When designing it is important to keep the equilibrium distance and pull-in voltage into account to prevent these event from happening.

$$x_{eq} = \frac{2}{3} x_0 \qquad u_{pi} = \sqrt{\frac{8Kx_0^3}{27\epsilon A}} \tag{9}$$

For a differential readout the combs are divided in two different capacitors. When there is movement the capacitance of one capacitor will increase and the other decreases. A principle of the operation is visible in Figure 5. The change in capacitance is given by equation 7.

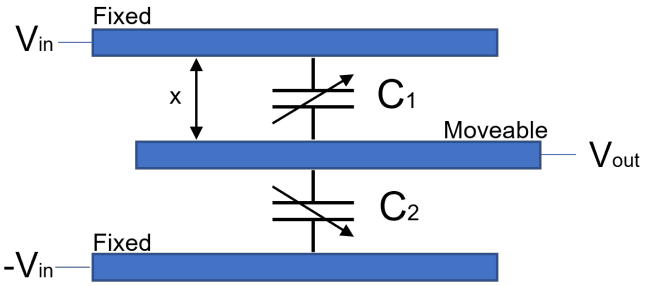

Fig. 5: Electrical operating principle of a differential capacitive readout

The capacitances C_1 & C_2 can be described as a constant part and a variable part. C_1 & C_2 are designed to be mirrored versions they have an equal capacitance in rest position, because of this the constant capacitance will be equal and will fall away because of the differential readout, as is visible in the following equations.

$$C_1 = C_1 + \Delta C_1 \qquad C_2 = C_2 - \Delta C_2 \tag{10}$$

$$C = (C_1 + \Delta C_1) - (C_2 - \Delta C_2) = 2\Delta C \tag{11}$$

The change in capacitance will be small (range of pF) and needs to be amplified, this is realised with a charge amplifier. The design and operation of this charge amplifier will be discussed later on when explaining the measurement setup. A simplified schematic is visible in Figure 6. What is of importance is that the charge amplifier works with a feedback capacitor (C_f), this capacitor will determine the gain of the amplifier and is important to get an expression for the output voltage.

$$V_{out} = \frac{C_1 - C_2}{C_f} \cdot V_{in} \tag{12}$$

The output voltage will be dependent on the difference between the capacitors and the feedback capacitor used for the charge amplifier, the lower limit of this feedback capacitor is $1pF$. Below that the capacitance comes in the region of parasitic capacitances present on PCBs and the capacitor would no longer have a significant effect.

After the charge amplifier a lock-in amplifier is used to demodulate the output signal from the carrier signal (V_{in}) that is used. The lock-in amplifier works by multiplying the signal with the reference carrier and then using a low-pass filter to remove the carrier from the output signal. The result is the output voltage created by the capacitance difference. Combining the different parts results in the schematic as it is visible in Figure 6.

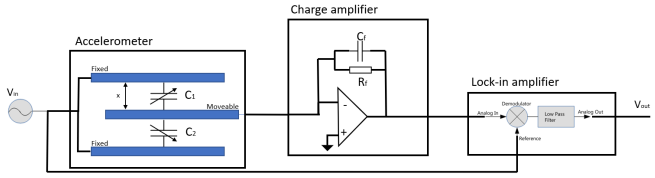

Fig. 6: Block diagram of the different steps performed in the measurement of an accelerometer.

D. Noise

Because of the small dimensions of accelerometers an important performance measure is the noise from thermal motion. The gas surrounding the mass of an accelerometer vibrates and causes movement of the mass. This is a limiting factor for the performance and is indicated with equation 13 [9]. This equation is often written in a different form by re-writing the equation for the quality factor (equation 2) and substituting this for the damping factor.

$$TNEA = \frac{\sqrt{4k_bTD}}{M} \qquad TNEA = \frac{\sqrt{4k_bT\omega_r}}{QM} \tag{13}$$

These equations give an indication for what can be done to improve the total noise equivalent acceleration (TNEA). One way would be to reduce the temperature (lower T) which would cause less vibrations in the surrounding gas. Another measure is to improve Q and M. The quality factor is dependent on the mass (M) but also on the damping factor. The quality factor would significantly increase if measurements would be performed in a vacuum. In this case the damping coefficient would be extremely low because there are almost no gasses to damp the movement of the mass.
Performing measurements at low temperatures or in vacuum both require a complicated measurement setup with controlled environments. They also would not resemble use of an accelerometer in the real world. Therefore, improving the TNEA is done best by designing a large proof mass.

Typically signals are converted to higher frequencies to improve the signal-to-noise ratio. For MEMS accelerometers it is typical to apply a carrier of 100kHz - 10 MHz. This same principle can be applied in an electromechanical way, using Electro Mechanical Amplitude Modulation (EMAM) [8].

EMAM works by oscillating a structure at a frequency that is significantly higher then the bandwidth of the sensor, up-converting the signal to a frequency that is less troubled by noise. Figure 7 shows how this looks in the frequency domain.

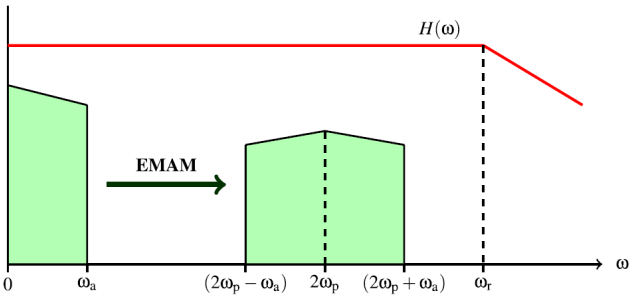

Fig. 7: Illustration of the EMAM principle in the frequency domain [8].

The red line indicates the resonance frequency of the oscillating structure. $2\omega_p$ is the frequency chosen for oscillation of the system. This frequency should stay well below the resonance frequency. The range $0 - \omega_a$ is the frequency range of the measured signal, which is up-converted around $2\omega_p$. Noise or other interferences that are located near the frequency range $0 - \omega_a$ are now of less significance on the signal.

For accelerometers the EMAM principle can be realised by oscillating the readout structure (the combs that typically are fixed to the reference frame) at a specified frequency. How this would look is illustrated by Figure 8, which illustrates a simplified version of the to be presented design. Actuation combs are connected to the readout structure. The blue

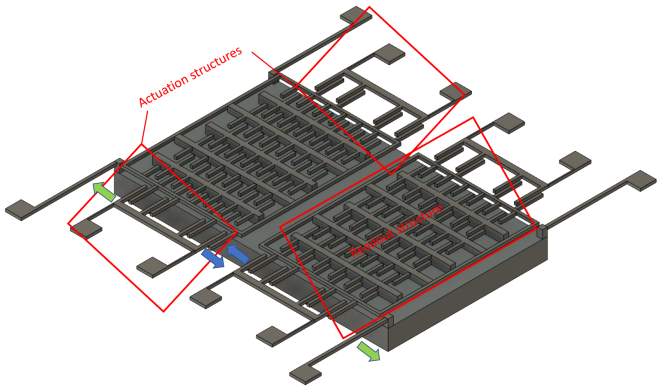

Fig. 8: Simplified 3D model of an accelerometer design with actuators to move the readout structure. The 3D model does not have accurate dimensions.

and green arrows indicate the direction of movement of the actuation. The two readout structures can be actuated independently. The colours of the arrows indicate how the actuators need to be operated. When actuated both the readout structures will move simultaneously in the direction of the green arrow and blue arrows respectively. The readout structure has a suspension consisting of springs that are independent from the springs and mass used for measuring acceleration. Because of this an additional mass-spring-damper system is created that has its own resonance frequency, mass, quality factor, spring constant and damping factor.

III. Design: Initial

The MEMS accelerometer is designed on a Silicon on Insulator (SOI) wafer, which is illustrated in Figure 1. The area for a microchip is $7.5\ mm \times 7.5\ mm$. As discussed in the theory the mass needs to be as large as possible, to reduce the TNEA (equation 13). This needs to be balanced with the spring constants and intended sensitivity and bandwidth. The goal of this paper is to properly design and implement the use of silicon nitride isolation trenches, not to create the most sensitive or most optimized accelerometer. The mass is chosen with dimensions of $5000\ \mu m \times 3300\ \mu m$, and the intended resonance frequency is around 1 kHz. The motivation for this is that there remains enough area on the chip to realise the actuation structures for the design with a moveable readout. And a resonance frequency around 1 kHz gives a good bandwidth for measurements and allows for reliable spring designs that take up little space. With the chosen area the total weight of the mass becomes $14.85mg$, this is including the readout fingers that will be connected to the mass.

A. Springs

To realise the resonance frequency of 1 kHz equation 2 is used to find the necessary spring constant. This is an iterative process because the mass is dependent on the size of the readout structure and will slightly change. The resulting required effective spring constant is $373.2N/m$. This effective spring constant is realised by using four identical springs that are placed in parallel. The design of the springs is kept simple and they are designed as rectangular beams. The dimensions of the springs are visible in Table I. Using equation 2 they result in the desired spring constant. Figure 9 shows how the springs look in the mask design and Figure 10 gives an indication of the location of the springs.

TABLE I: Spring dimensions and resulting spring constant for individual springs.

Dimension	Value	Unit
Length	250	μm
Width	7	μm
Height	25	μm
Spring constant	93.3	N/m

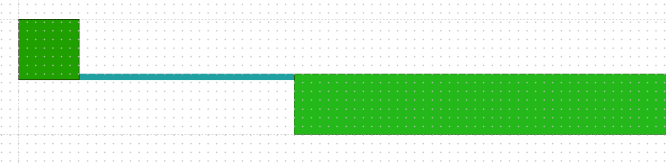

Fig. 9: Snapshot of Clewin5. Illustration the mask design of a single spring. Green indicates an anchor or connection to the mass. Blue is the actual spring.

B. Readout

A part of the mass of $14.85\ mg$ consists of the readout structure that is designed in the device layer and is fixed to the mass. The dimensions of the fingers used in the readout are visible in Table II. The fingers are connected with a structure of horizontal and vertical beams that create a grid. This grid is suspended above the mass. Figure 10 gives an indication of how the chip will look with the readout structure suspended above the mass.

TABLE II: Dimensions of the fingers that make up the parallel plate capacitors

Dimension	Value	Unit
Length	250	μm
Width	5	μm
Height	25	μm
Overlap	235	μm

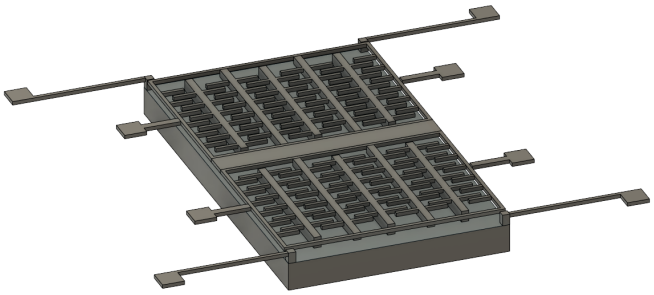

Fig. 10: Simplified 3D model of the readout structure of the initial accelerometer design. The model does not have accurate dimensions and is only for illustration of the operating principle.

The readout structure that is suspended above the mass makes this design stand out, it also makes designing this accelerometer a challenge because the readout structure has a large area and needs to be suspended properly. The support of the readout structure consists of a grid of 4 long vertical support beams and a thick horizontal support beam. These support beams are connected at the top with anchor points that are connected to the substrate. Connected to vertical support beams are the readout fingers that make up the parallel plate capacitors. Normally the entire readout structure is electrically connected to each other, this would not result in a differential capacitive readout. Zooming in on the horizontal support it actually consists of 2 parts that are separated with a long SiN trench, as is visible in Figure 11. The horizontal beam is connected to the substrate at both ends. With the implementation of the SiN trench two capacitors are created. The fingers within one capacitor all have the same configuration. The other capacitor is a mirrored version.

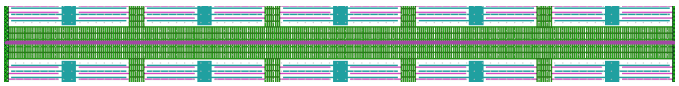

Fig. 11: Snapshot of Clewin5 zooming in on the horizontal support of the readout structure which used the SiN trench technology to isolate electrical areas. Dimensions of the SiN trench are enhanced for a clear illustration.

Using this structure a total of 1540 parallel plate capacitors are realised above the mass. The fingers that make up a parallel plate capacitor are 5 μm apart in the neutral position. The parallel plate capacitors are 15 μm apart from each other. This creates an optimal use of the area with a maximum readout. A more detailed explanation is discussed in Appendix A.

Apart from the capacitance between the parallel plates there are also capacitances between other parts of the readout structure. All the areas that of the readout structure that have a potential difference will become capacitors. To get an accurate value for the total capacitance all these areas need to be taken into account. Each capacitor that is formed can be described with equation 7. A complete breakdown of all the capacitances is given in Appendix B.

The capacitances can be separated in two categories, constant capacitances (independent of movement in desired direction) and variable capacitances (dependent of movement in desired direction). All the variable capacitances need to be taken into account to form an expression for the change in capacitance. This results in Equations 14 & 15 respectively:

$$C_1 = \frac{\#\ fingers}{2}\left(\frac{\epsilon A}{d_0 + x} - \frac{\epsilon A}{d_1 - x}\right) \tag{14}$$

$$C_2 = \frac{\#\ fingers}{2}\left(\frac{\epsilon A}{d_0 - x} - \frac{\epsilon A}{d_1 + x}\right) \tag{15}$$

The equations are an adaptation from Equation 7. Added symbols are d_0 which is the initial distance between a parallel capacitor plate ($5\mu m$), d_1 is the initial distance the next parallel capacitor pair ($15\mu m$), A is the overlapping area of the parallel capacitor pairs nad $\#\ fingers$ is the number for the 1540 realised parallel plate capacitors. The resulting output capacitance is given by $C_1 - C_2$, the result is visualised in Figure 12.

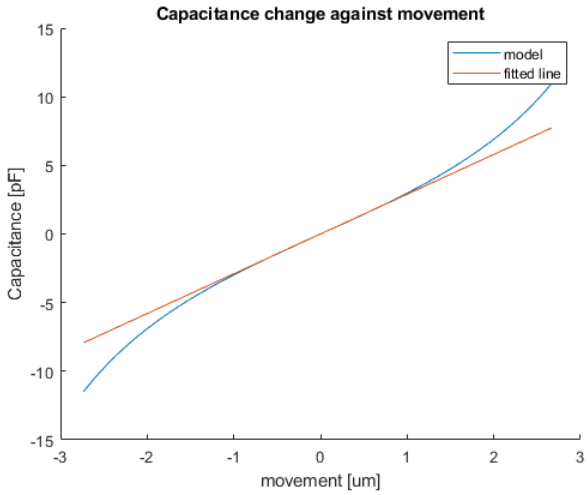

Fig. 12: The change in capacitance against the movement of the mass. The blue line indicates the capacitance behaviour. The red line is a linear fit to display the linear behaviour for small movements.

Figure 12 shows a fitted line, this line has a slope of 2.9 $pF/\mu m$ which is the sensitivity of the linear part of the accelerometer. The linear part is roughly up until movements of 1 μm. To put this in perspective, a force of approximately 2.5 G will cause a movement of 1 μm.

Due to the differential readout and the symmetrical design of C_1 & C_2 the constant part of the capacitance is eliminated. But it is important to look at the total capacitance, and to be aware of the parasitics. Combining all the constant parasitic capacitances results in a value of 11.3 pF for C_1 & C_2

individually. In rest position the variable capacitance of C_1 & C_2 equals 10.7 pF. The total capacitance of C_1 & C_2 becomes 22 pF.

Filling in the dimensions of the parallel plate capacitors (Table II) in equation 9, results in the pull-in voltage which is 18.6 V. From the same equation 9 we find that the equilibrium distance is 3.33 μm. The equilibrium distance leaves a range of 1.6 μm to safely operate the accelerometer. From Figure 12 we see that a movement of 1.6 μm already falls outside the linear range, most likely the accelerometer will not be operated near this limit. Next to that the 18.6 V gives a large range for the readout to be supplied.

To prevent exceeding this equilibrium distance stoppers are designed. If pull-in would occur these stoppers, which are made of SiN prevent the parallel plates from completely touching each other. When the electric signal is removed the plates can return to their initial position and won't remain stuck to each other. The stoppers are located at the anchor points for the support structure, as is visible in Figure 13. The blue structure surrounding the anchors is connected to the mass and follows the same motion. If the structure touches the stoppers the fingers will not be able to move further.

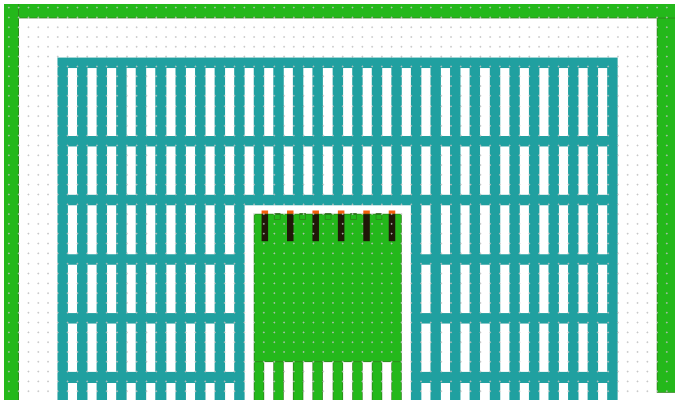

Fig. 13: Snapshot of Clewin5. Zooming in on the Silicon Nitride trenches that act as stoppers. They prevent the capacitor plates (fingers) from snapping together (pull-in).

The complete mask design of the initial accelerometer design is visible in Appendix C. Table IV summarises the important properties from the final design.

IV. Design: Movable readout

A second accelerometer design is created, this design continuous on the initial design but has a few unique differences. The second design has a completely movable readout structure, to realise an EMAM oscillation. The dimensions of the readout structure are kept the same, which results in a structure with the same amount of readout fingers. The support structure changes slightly due to the movable nature but this has minimal changes on the capacitance.

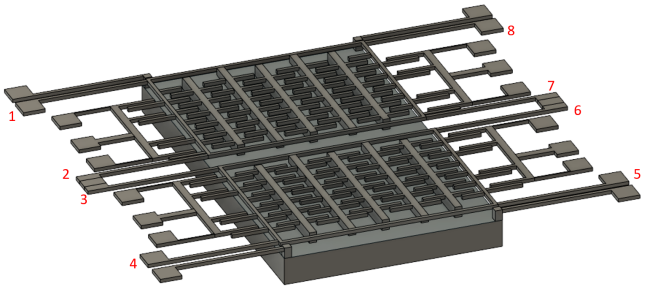

Fig. 14: Simplified 3D model of the accelerometer design with a moveable readout. The model is not to scale and only used for illustration of the design.

The difference of this design is that with the help of actuators the sensing fingers can be moved. By applying an alternating signal to the actuators the sensing fingers are brought in an oscillating movement of approximately 10 kHz. To be able to design this, the Silicon Nitride isolation trenches are critical. With the use of these trenches areas of the microchip can be electrically isolated from each other. This enables the actuation structure to be supplied with an actuation signal without influencing the readout. It also provides new opportunities for creating a better support system for the readout structure by using isolating elements.

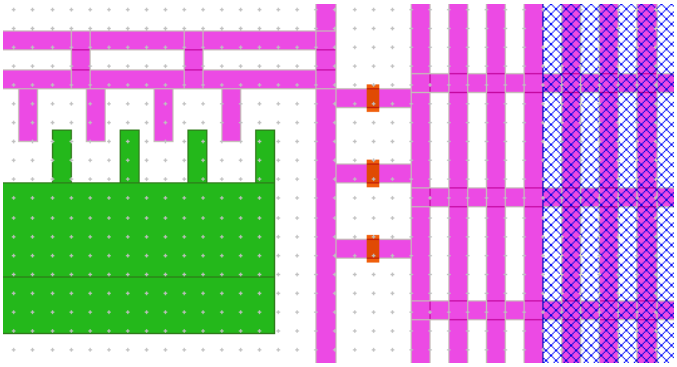

Fig. 15: Snapshot of Clewin5, zooming in on the Silicon Nitride trenches that isolate the actuation from the readout. The trenches are indicated in orange. Green indicates silicon that is fixed. Pink indicates silicon that will be free to move.

Figure 14 shows the simplified 3D model of the design with a moveable readout. Figure 15 zooms in on the mask design of the Silicon Nitride isolation trenches (indicated with orange) that isolate the actuation structure from the readout structure.

To make the entire structure freely moving extra springs are used. First there are eight springs that connect to the support structure of the readout fingers. Their dimensions are visible in the top part of Table III. The springs are located at the

corners and at the sides of the horizontal support beam. They are indicated with the numbers 1 - 8 in Figure 14. To provide extra support each finger of the actuation combs has a spring with a very low spring constant. The dimensions are visible in the middle part of Table III. The mask design of this spring is visible in Figure 16. Over here the SiN technology is used to prevent the electrical signal from reaching the actuation comb through the spring.

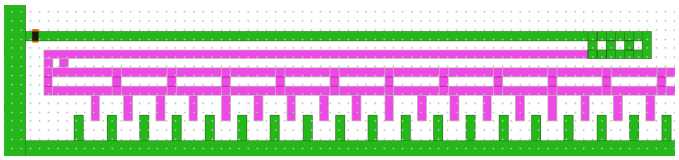

Fig. 16: Snapshot of Clewin5 zooming in on the spring design for the actuation combs. Purple indicates the moveable part. Green is fixed to the reference frame.

The resulting spring constants and total actuation spring constant are also listed in Table III. The complete design of this accelerometer consists of three independent mass-spring-damper systems. First, the mass with the suspension springs as was already discussed in the initial design. But with the moveable readout and different suspension both C_1 & C_2 become independent mass-spring-damper systems. There designs identical so they will behave the same. The 'spring constant actuation' and 'resonance frequency actuation' in Table III give the corresponding values. The important properties of the eventual design are listed in Table IV.

TABLE III: Dimensions and resulting spring constants for the actuation structure.

Dimension	Value	Unit
Suspension spring		
Length	275	μm
Width	8	μm
Height	25	μm
Spring constant	104.63	N/m
Actuation comb spring		
Length	300	μm
Width	5	μm
Height	25	μm
Spring constant	9.84	N/m
Amount of suspension springs	4	
Amount of actuation springs	50	
Total spring constant	910.42	N/m

TABLE IV: Important properties of the resulting design with a moveable readout.

	Value	Unit
Weight Mass	15.9	mg
Weight readout	0.40	mg
Spring constant Mass	373.18	N/m
Spring constant actuation	910.42	N/m
Resonance frequency Mass	771.59	Hz
Resonance frequency actuation	10779.17	Hz

The design with the moveable readout uses the same dimensions and properties for the readout as the initial design. Because of this all the electrical properties like the pull-in voltage, equilibrium distance and expected capacitance output are equal. Stoppers are harder to design because the readout structure is now also moving. By carefully tuning this movement, and the use of an AC signal should prevent pull-in from occurring.

V. Simulations

By implementing the theory and the design simulations can be performed to visualise the behaviour and expected outcome of both the accelerometer designs. The simulations are performed in Simulink in combination with MatLab. A complete overview of the Matlab code and Simulink model is visible in Appendices H & G.

The simulations are build up of different parts. First there is the actual conversion of acceleration (a) to displacement (x). This is described with the spring-mass-damper model, which is a second order differential equation described by equation 1. This equation can be modelled and the parameters, mass (M), damping (D) and spring constant (K) are inserted. To determine the damping equation 2 is re-written and a quality factor (Q) of 10 is used. Figure 17 shows the implementation of the simulink model.

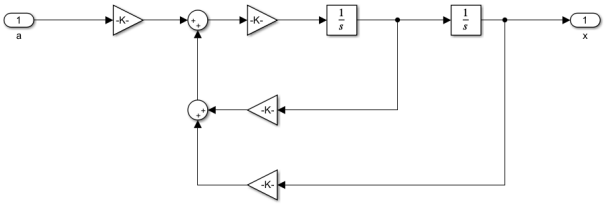

Fig. 17: Snapshot of simulink showing the model of the second order differential equation for a mass-spring-damper system.

Figure 18 shows the result for a sudden input of 1G. Clearly visible is the oscillation that occurs at the input of 1G. The oscillation damps out after a few cycles. From this behaviour it can be concluded that the system is underdamped.

Critical damping would occur for a damping ratio of 1 (or close to one). The critical damping coefficient is given by:

$$c_c = 2\sqrt{KM} \tag{16}$$

Which equals 0.154 for this design. The chosen damping factor is 0.0077, which is significantly lower but corresponds to the quality factor of 10.

The simulated movement of the mass is inserted into the next block of the simulation. The conversion from movement to a capacitance. This simulates the operation of the readout structure. The blocks capacitance 1 & capacitance 2, which are visible in Figure 19 use equations 14 & 15 for calculating the capacitances. The results of these blocks are combined

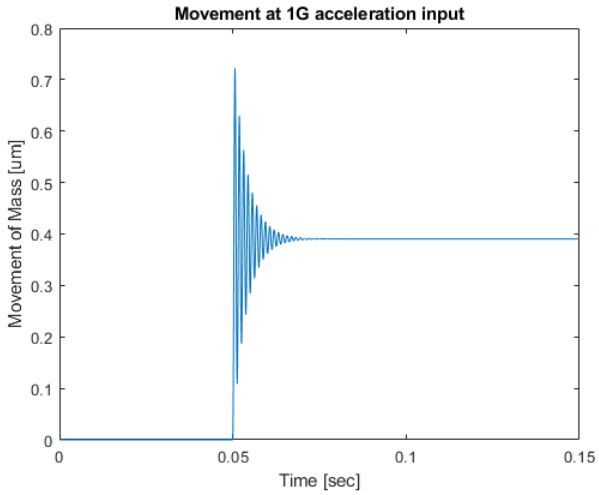

Fig. 18: Resulting movement of the simulation for an acceleration pulse of 1G.

with an electronic carrier signal with a frequency of 100 kHz.

The functioning of the charge amplifier is simulated by building equation 12 with a sum to combine the signals from C1 & C2 and a gain block. After that the signal needs to be removed from the carrier signal again. In the measurements this is done with a lock-in amplifier, this is simulated by multiplying with the carrier and using a low pass filter. The low pass filter is a 8th order Chebyshev filter with a cut-off frequency around 1.1 kHz. Frequencies above the cut-off frequency are beyond the bandwidth of the accelerometer. The resulting system for the simulation of the initial design is visible in Figure 19.
The output for a step response is visible in Figure 21.

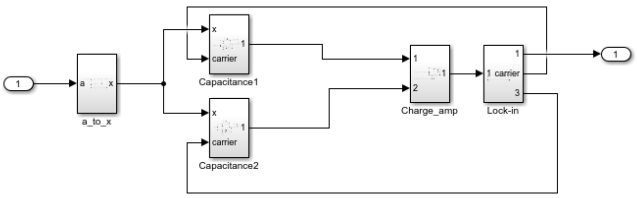

Fig. 19: Snapshot of Simulink showing the subsystems for the model of the initial accelerometer design.

The simulation for the design with the moveable readout requires some extra steps to properly simulate the behaviour. For this design the signal needs to be mechanically oscillated with the intended 10 kHz. For simplicity the oscillation is assumed to be ideal and simulated with a sine wave. The extra modulation step requires an additional demodulation. Therefore the cut-off frequency off the electrical modulation is chosen around 11 kHz, so that the mechanical modulation is not removed by this filter step. The second low pass filter is similar to the one of the initial design and has a cut-off frequency around 1.1 kHz. Figure 20 shows the resulting system for the moveable readout. Both the filters used for this simulation are 8th order Chebyshev filters.

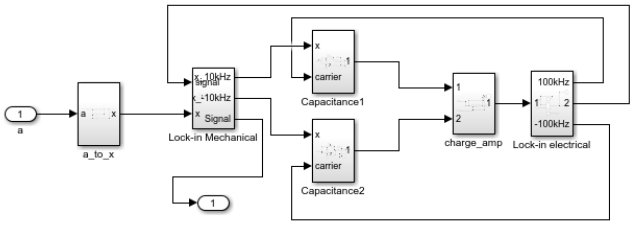

Fig. 20: Snapshot of Simulink showing the subsystems for the model of the moveable readout accelerometer design.

Both designs are first tested for normal operation by applying the same signal. The previously used step function is used to create a sudden input of 1G. Figure 21 shows the result, the top graph is the input, the middle graph is the output of the initial design and the bottom graph shows the output of the design with a moveable readout. From these results we see that both designs show the desired output that follows the input. Differences are that there seems to be more filtering for the design with the moveable readout, which is logical since there are two demodulation and low-pass filter steps. Because of this additional filtering the output of the second design is also lower. This does have an influence of roughly a factor 20. But the output of the moveable readout design would still easily be measurable.

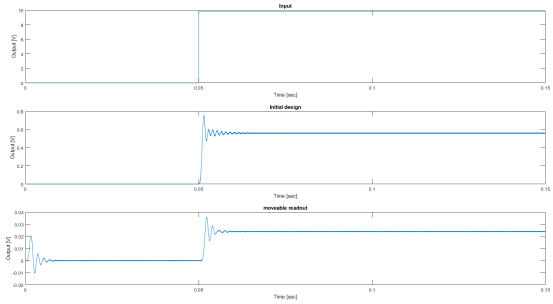

Fig. 21: Simulation results for a 1G acceleration input. Top is the input, middle is the initial design and bottom is the moveable readout design

More interesting is what happens when the situation is not ideal. This is simulated by introducing a parasitic source with a random signal, as is visible in Figure 22. This random signal has the same amplitude as the output of C_1 or C_2. Figure 23 shows the results of both the outputs. Looking at these results we see that both of them are influenced by the parasitic capacitance. But output of the design with the moveable readout still follows the behaviour of the input.

When looking closely the initial design still shows that it follows the input behaviour, but the signal is heavily biased and the noise is in the same order of magnitude as the signal. This shows promising results that the extra modulation reduces the influence of parasitic sources.

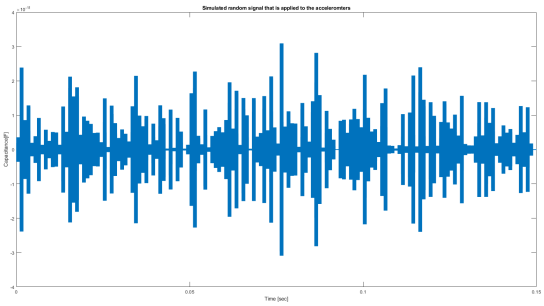

Fig. 22: Simulated random signal applied to the accelerometer simulations to simulate a parasitic capacitance.

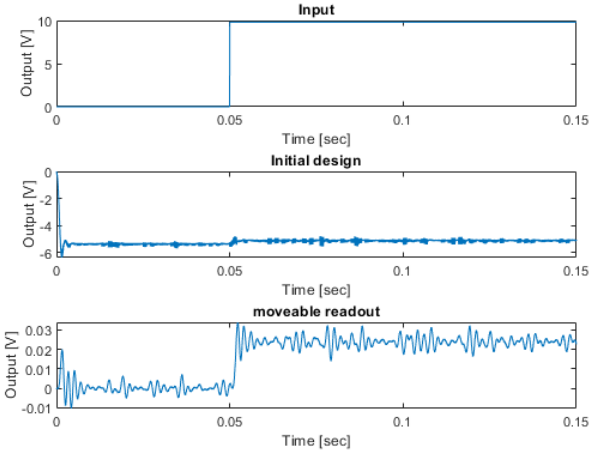

Fig. 23: Simulation results for a 1G acceleration. With an additional simulated source of parasitic capacitance.

A frequency analysis is performed to see how much unwanted signals are suppressed, and give more insight in the performance of the accelerometers. The step response input is replaced by a periodic input of a sine wave with an amplitude of 2G and a frequency of 600 Hz.

Figure 24 shows the complete frequency spectrum for the ideal measurement without any noise. The yellow signal is the response for the initial design. The blue signal is the response for the design with the moveable readout. Both designs show a high peak near 0 Hz. And a peak or several peaks around 200 kHz.

Figure 25 zooms in on the frequency range of 0-10kHz, and shows that the peak is actually at 600 Hz, which is the input frequency. Back to Figure 24 we also see a large peak at 200 kHz for the initial design and several peaks surrounding the 200 kHz for the design with the moveable readout. The fact that this peak occurs at 200 kHz and not the expected 100 kHz is probably due to aliasing. The same effect that causes the multiples of the 600 Hz to show small peaks.

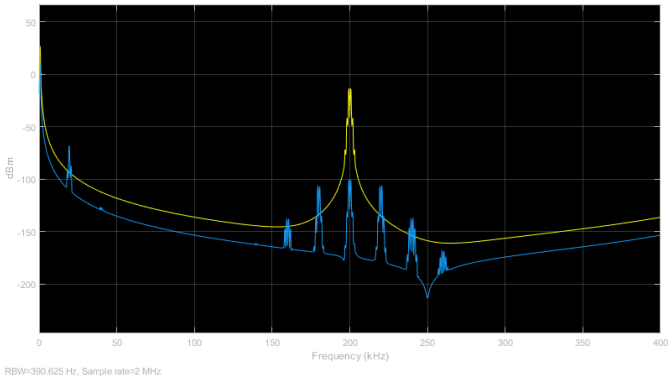

Fig. 24: Snapshot of the spectrum analyzer in Simulink. This is the full frequency range with no noise applied. Yellow shows the frequency response for the initial design. Blue shows the frequency response for the design with the moveable readout.

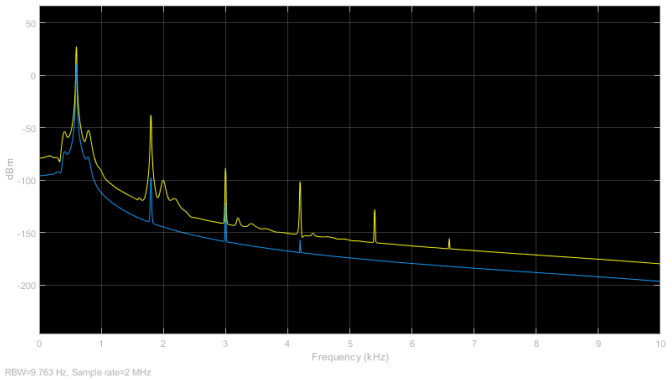

Fig. 25: Snapshot of the spectrum analyzer in Simulink. This is for the frequency range 0-10 kHz with no noise applied. Yellow shows the frequency response for the initial design. Blue shows the frequency response for the design with the moveable readout.

Now looking at the situation where noise is applied. In Figure 26 we see the results for the full frequency range. The initial design shows higher peaks at multiples of the 100 kHz carrier. The response of the moveable readout shows more of the influence of the 10 kHz mechanical carrier, but the signals are heavily suppressed.

Zooming in again on the range of 0-10 kHz, visible in Figure 27, we see that the response for the design with the moveable readout hardly changed. While the response of the initial design shows much more disturbance. Which is very promising for the functioning of the EMAM.

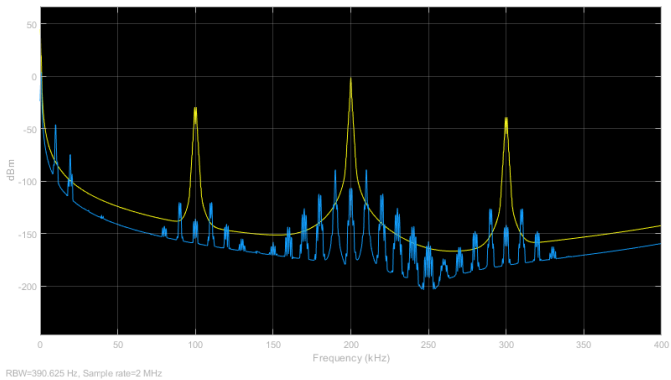

Fig. 26: Snapshot of the spectrum analyzer in Simulink. This is the full frequency range with noise applied. Yellow shows the frequency response for the initial design. Blue shows the frequency response for the design with the moveable readout.

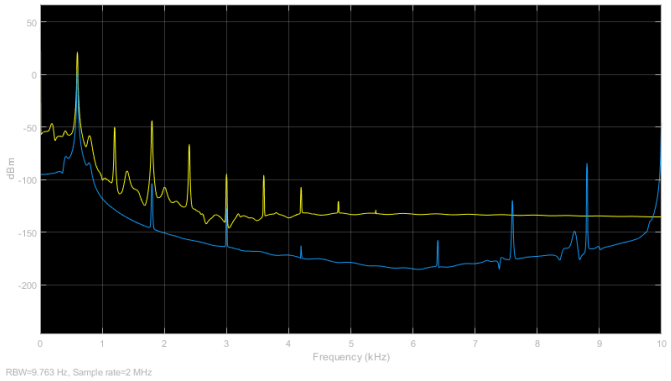

Fig. 27: Snapshot of the spectrum analyzer in Simulink. This is for the frequency range 0-10 kHz with noise applied. Yellow shows the frequency response for the initial design. Blue shows the frequency response for the design with the moveable readout.

VI. Fabrication

As mentioned the wafers used in the fabrication process are Silicon-On-Insulator, as is visible in Figure 1. To fabricate the microchips several techniques and steps are necessary. Materials like silicon oxide (SiO_2) and the silicon nitride need to be deposited. Detailed structures need to be etched, which is done with Deep Reactive Ion Etching (DRIE). Vapour-HF etching is used for isotropic etching of the sacrificial silicon oxide layer. Several masks are required for completing the process, in this case a mask for the device layer, a mask for the handle layer and a separate mask for creating the Silicon Nitride trenches. The masks are designed in Clewin5 and are visible in Appendix C.

The first mask that is applied is that for the Silicon Nitride trenches. Design rules for the trenches are that they can not be wider than $3\mu m$. To make sure that they are isolating it is best to make them a bit longer to make sure that the surrounding structures are isolated by the trench (this is visible for the isolating structures in Figure 15.

The second mask is that of the device layer. The most important design rules of this layer are the minimum feature size of $3.5\ \mu m$. And the underetch of the buried oxide layer (BOX), which in the order of 5 to 10 μm. Structures that must be released from the substrate should be smaller than $10\ \mu m$. There is a gray area for the etching from 10 to 50 μm. If a structure must stay fixed to the substrate it is safest to make it at least $50\ \mu m$ wide.

The third mask is for the handle layer, which normally is only used for releasing the chip. In this case the formation of the mass will also happen in this step. Because of the height of the handle layer ($380\ \mu m$), trenches of $90\ \mu m$ are needed to reach the BOX layer and guarantee a good release. An effect that should be taken into account is that the trenches in the handle layer will not be as straight, this can cause the mass to have a slightly different shape and therefore different mass and resonance frequency. The difference is probably of such a low magnitude that it is not noticeable during measurements.

The complete process is very detailed and needs to be performed for a specified duration with precise concentrations of materials at certain temperatures [13]. The key steps are listed below.

1) Grow thin layer ($2\ \mu m$) silicon oxide
2) Apply photoresist
3) Expose photoresist
4) Etch silicon oxide layer to transfer structures from photoresist to oxide layer
5) DRIE etching to create structures in the silicon
6) Strip photoresist and clean the wafer removing any additional protection layers
7) Vapour HF etching to remove the silicon oxide layers and release the structures in the device layer

The fabrication process is performed at the Nanolab at the University of Twente by qualified specialists that are trained for properly using the machinery and can perform the necessary recipes for creating microchips with minimal risks of failure.

VII. Measurement setup

As discussed before, the accelerometer requires external electronics in order to function properly, as indicated by Figure 6. Therefore the bondpads of the microchip connect to a PCB which contains the extra electronics or enables connections to external equipment.

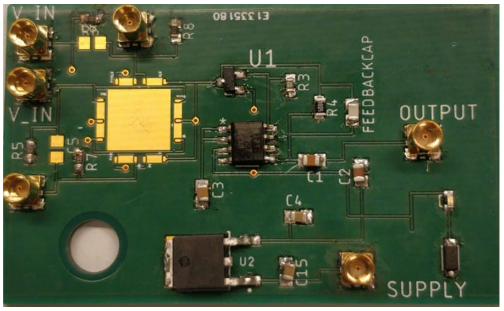

Fig. 28: Picture of the PCB, showing the location of the microchip, the coax connectors and the electronics used for the amplifier circuit.

The PCB, which is visible in Figure 28, connects the chip to an amplifier circuit which provides a measurable output signal. The PCB also creates connections to the power supply, function generators, an oscilloscope and a lock-in amplifier. Together this equipment makes up the measurement setup. Placing the amplifier circuit close to the chip not only reduces the amount of wire connections but also prevents signal losses before the signal is amplified.

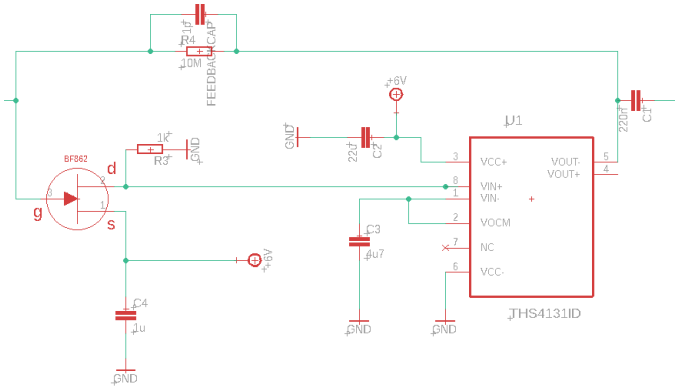

Fig. 29: Schematic of the amplifier circuit located on the PCB.

Figure 29 shows the schematic of the amplifier circuit that is used. The electronics consist of a JFET and a charge amplifier. The charge amplifier produces an output voltage which is inversely proportional to the reference capacitor, as we already saw in equation 12. The value of this reference capacitor determines the gain. For the measurements on the accelerometer chips the value of the reference capacitor is 1 pF. The amplifier circuit is powered by a linear voltage regulator that is powered by an external power source. To indicate that the amplifier is turned on a LED is located on the PCB.

Figure 30 shows a schematic of the complete measurement set-up and how all the equipment is connected to the PCB. The advantage of the small PCB is that it can be directly mounted on the shaker that is used in the measurement set-up to create accelerations.

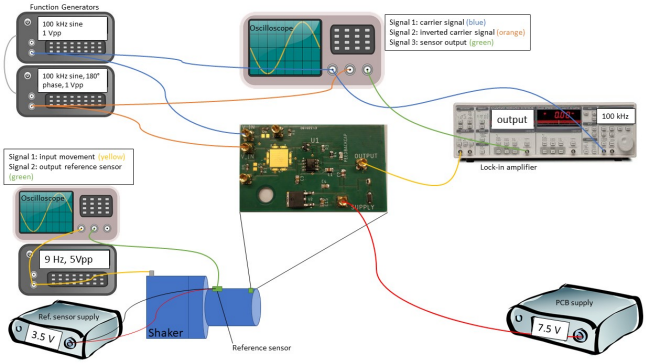

Fig. 30: Schematic of the entire measurement setup. Indicating all the external equipment that is used, for what purpose, and how it is connected to the microchip via the PCB.

The reference sensor used in this measurement setup is a ADXL354 [14]. The output of the reference sensor is an analog voltage that can be connected directly to the oscilloscope, which visualises the output of the reference sensor. What the oscilloscope shows is the input frequency of the shaker, and the amplitude of the reference signal. The amplitude of the reference signal translates to an acceleration. When an accelerometer chip is connected to the measurement setup it shows the same two things. The output frequency follows the frequency of the input of the shaker, and the amplitude of the output is a measure for the corresponding measured acceleration.

This measurement setup can be used for the characterisation of measured accelerometers. Static measurements, with a constant acceleration, can be used to obtain information like the sensitivity, offset, range and accuracy of the measured accelerometer. And dynamic measurements give insight in the frequency behaviour of the measured accelerometer and can be used to find the bandwidth and quality factor of the accelerometers.

VIII. Results

Before proceeding to the results it must be noted that during the fabrication process the etching machine broke down and the fabrication of the proposed accelerometer designs could not be completed. This had several consequences for the remainder of the research. The simulations are used to visualise the behaviour of the proposed accelerometer designs. The measurement setup is still built and tested. For the testing, generic accelerometer microchips are used. These chips are compared to the proposed designs to get an indication of the expected result if the measurement setup would be used with the designed accelerometers.

A. *Measurement setup*

Figure 31 shows the realisation of the measurement setup. This setup is built according to the schematic of Figure 30.

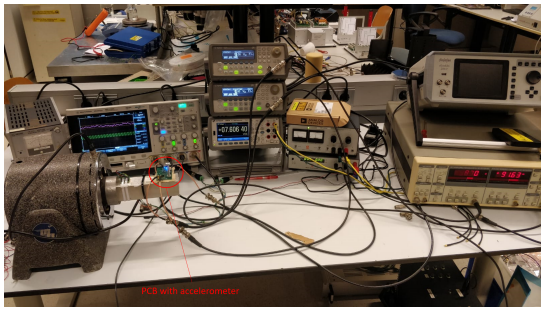

Fig. 31: Realisation of the measurement setup, showing all the equipment and the cables connecting to the PCB mounted on the shaker.

Before connecting an accelerometer chip the functionality of the PCB was tested, this was done by replacing the microchip with two capacitors with an equal value. These capacitors were connected to the two inputs and the output of the microchip. Now by connecting the measurement setup the expected output is a flat line, since the capacitances are equal. Figure 32 shows the result of this experiments which shows a flat line. Next the amplitude of one of the input signals was changed, this should change the output on of the capacitors showing a result from the differential pair. This result is visible in Figure 33 which shows that the influence of one capacitor increased.

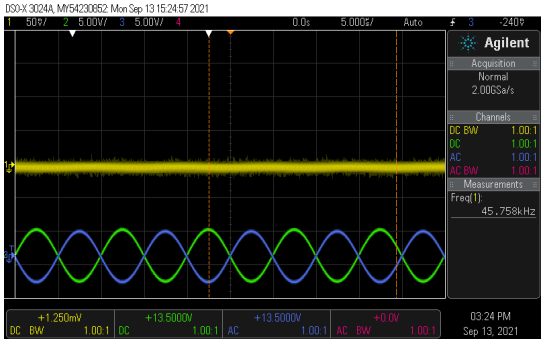

Fig. 32: Screenshot from the oscilloscope. Green and blue show the input signals with an equal amplitude. Yellow shows the output of the differential pair.

With the PCB tested an accelerometer microchip was connected. The result of this is visible in Figure 34, which shows the output of the accelerometer chip (pink) and the reference sensor (green). Visible is that both signals show the $3.6Hz$ input signal of the shaker that was used. The reference sensor shows an amplitude of $60mV$ and the measured accelerometer shows an amplitude of $350mV$. The signal does show a significant influence of noise compared to the output of the reference sensor. This effect can possibly be reduced by using additional filtering after the lock-in amplifier.

Unfortunately the functioning of this microchip was of a short duration. The output visible in Figure 34 could not be reproduced. No further measurements could be performed.

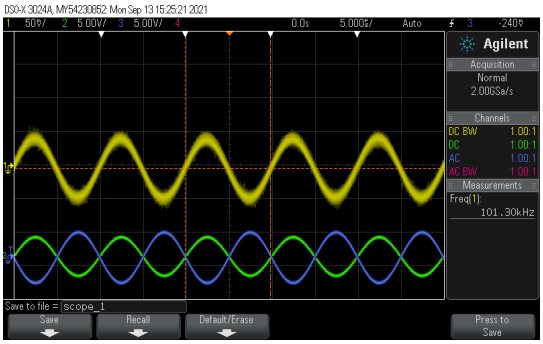

Fig. 33: Screenshot from the oscilloscope. Green and blue show the input signals with a difference in amplitude. Yellow shows the resulting output of the differential pair

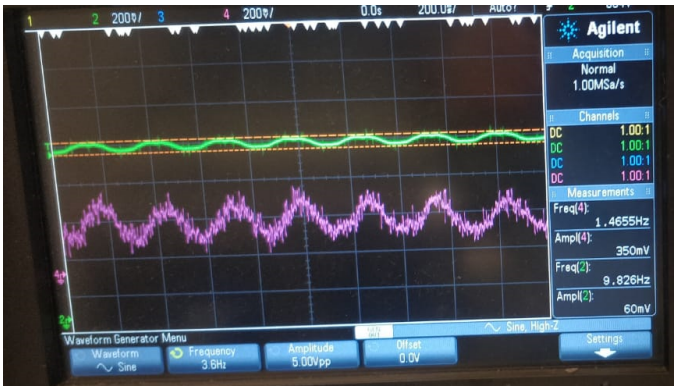

Fig. 34: Screenshot from the oscilloscope. Green shows the output of the reference sensor. Pink shows the output of the measured accelerometer chip. Note that the measured frequencies from the oscilloscope are not accurate.

Because of this no quantitative information about the measured accelerometer could be obtained.

B. validation chip design

Due to the circumstances in the Nanolab no tests can be performed on the designs of the microchips presented in this paper. To get an idea of the expected output the designs of the microchips can be compared to the microchip used for validating the measurement setup.

The chip used, visible in Figure 35 was only connected with two readout combs and a connected for the output connected to the mass. Table V shows the dimensions of the readout structure of the chip used. With the connected combs there were 180 parallel plate capacitors. Each capacitor consists of 90 finger pairs.

The resulting capacitance change is visible in Figure 36 and has a sensitivity of $0.1pf/\mu m$. This sensitivity would be doubled when the entire chip would be connected but would still be a factor 10 lower compared to the expected results in Figure 12.

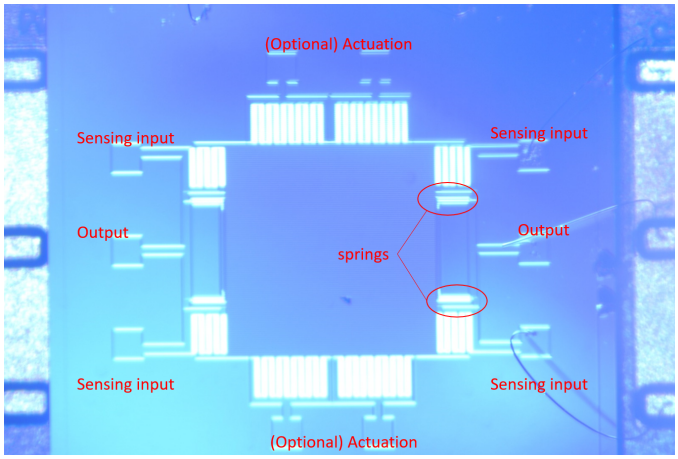

Fig. 35: Photo of the ship used in the measurements. Showing the layout and various bondpad locations of the microchip.

TABLE V: Dimensions of the fingers that make up the parallel plate capacitors.

Dimension	Value	Unit
Length	70	μm
Width	5	μm
Height	25	μm
Overlap	60	μm

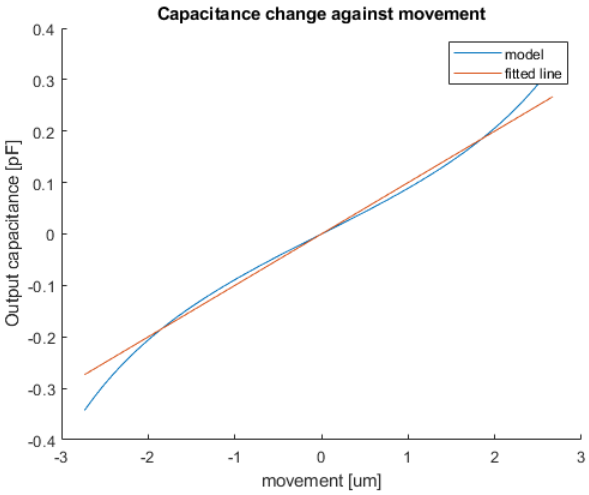

Fig. 36: Estimated capacitance results based on the design of the accelerometer chip used for measurements.

IX. Discussion

First it must be noted again that the biggest recommendation for future work is to fabricate the chips so that they can be tested and characterised.

Another point of discussion is the design and fabrication of the PCB's. There is definitely an advantage to using a small PCB with the amplification electronics as close as possible. In the design phase the decision was made to use only surface mount components to keep the bottom of the PCB flat for easy mounting to the shaker. During fabrication and testing it turned out that the coax connectors are very hard to properly connect surface mounted, they kept separating from the PCB sometimes destroying electrical traces in the process. The challenges in the fabrication of the PCB slowed down the validation of the measurement setup because there was an uncertainty in the functioning of the PCB. A possible future iteration could perhaps be designed with through hole components at the edges to make sure that it can still easily be mounted.

When looking at the measurement setup as a whole it still needs future work. All the individual components are tested and the measurement setup as a whole should work. However the desired output was realised only once and could not be reproduced afterwards. During testing several things came to light that could be the cause of this. During measurements a noticeable effect was that there was a stress on the coax connectors because of the weight of the cables hanging down, the fact that there is a stress there means that the cables were influencing the movement of the PCB and altering the results. Another thing is that the lock-in amplifier already displayed a signal in the range of 10-100 mV when no chip was connected. This interference possibly disturbed the output of the accelerometer and caused no clear frequency to be visible. This could be tested by using a different lock-in amplifier. The wirebonds turned out to be very fragile, a few times the wirebonds released from the PCB during operation of the shaker. Most likely this is a coincidence. The combination of these uncertain factors, and the pressure of a time limit were the cause that no solution for the malfunction of the measurement setup could be found.

Lastly the simulations, these were performed at a late phase in the research. The Simulink model is correct and representative for an accelerometer with measurement setup but could definitely be improved. At the moment the actuation of the second design is assumed to be ideal and simulated with a sine wave. In reality the actuation is a second mass-spring-damper system and there will be some oscillation and non-idealities when actuating. Also the demodulation and filtering stage is chosen at general values to give a good result for several scenario's. The filtering can be improved and altered to fit the range of the accelerometer better and give a good output result.

X. Conclusion

In this research two accelerometer designs are presented which implement Silicon Nitride isolation trenches in their designs. The first design used the isolation trenches to create more mechanical support without creating electrical connections. This enabled the design of a large readout structure suspended above a larger mass. Next to that the Silicon Nitride trenches are used as stoppers to prevent the parallel plates from collapsing onto each other in case of pull-in.

The second design uses the Silicon Nitride trenches at critical positions to isolate electric signals. In this case there is less mechanical support but the isolation enables the use extra electrical signals. With this method a readout structure is designed that can be actuated with an independent signal. This creates an accelerometer with both a mechanical and electrical modulation. This is similar to the EMAM principle. The combination of the modulations makes the accelerometer less vulnerable to outside parasitic sources.

Both accelerometer designs show an expected sensitivity of $2.9pf/\mu m$ which a factor 10 higher compared to the 'generic' accelerometer used during testing. This shows that the proposed design for using the entire area above the mass for readout results in a significant increase in sensitivity.

The accelerometer designs are simulated in Simulink and the results show that the double modulation makes the accelerometer less vulnerable to outside parasitic sources. There is still an influence which distorts the signal but the input signal could still be recovered. The frequency spectrum also shows that unwanted frequencies are suppressed further compared to the initial accelerometer design.

A measurement setup is built to test and validate the proposed accelerometer designs. Individual components from the measurements setup are tested and the measurement setup is working as intended. Unfortunately the expected output of a measured accelerometer was only obtained once and could not be reproduced afterwards. Because of this no quantitative data of the measured accelerometer is obtained. As discussed this needs further work.

Unfortunately the designed accelerometers could not be fabricated. Because of this the proposed accelerometer designs cannot be tested and validated. But a theoretic comparison with the 'generic' accelerometer used for testing shows that the expected output is higher and therefore we can conclude that the design is very promising for future work.

References

[1] C. Song, B. Ha, and S. Lee, "Micromachined inertial sensors," *IEEE International Conference on Intelligent Robots and Systems*, vol. 2, no. 8, pp. 1049–1056, 1999.

[2] N. Gupta, S. Dutta, A. Panchal, I. Yadav, S. Kumar, Y. Parmar, S. R. K. Vanjari, K. K. Jain, and D. K. Bhattacharya, "Design and fabrication of SOI technology based MEMS differential capacitive accelerometer structure," *Journal of Materials Science: Materials in Electronics*, vol. 30, no. 16, pp. 15 705–15 714, 2019. [Online]. Available: https://doi.org/10.1007/s10854-019-01955-0

[3] M. Benmessaoud and M. M. Nasreddine, "Optimization of MEMS capacitive accelerometer," *Microsystem Technologies*, vol. 19, no. 5, pp. 713–720, 2013.

[4] M.-h. Tsai, Y.-c. Liu, and W. Fang, "A Three-Axis CMOS-MEMS Accelerometer," vol. 21, no. 6, pp. 1329–1337, 2012.

[5] X. Zhou, L. Che, S. Liang, Y. Lin, X. Li, and Y. Wang, "Design and fabrication of a MEMS capacitive accelerometer with fully symmetrical double-sided H-shaped beam structure," *Microelectronic Engineering*, vol. 131, pp. 51–57, 2015. [Online]. Available: http://dx.doi.org/10.1016/j.mee.2014.10.005

[6] B.A.Boom, "Acceleration sensing at the nano-g level," 2020.

[7] J. W. Judy, "Microelectromechanical systems (MEMS): Fabrication, design and applications," *Smart Materials and Structures*, vol. 10, no. 6, pp. 1115–1134, 2001.

[8] H. Droogendijk, R. G. Sanders, and G. J. Krijnen, "Uncovering signals from measurement noise by electro mechanical amplitude modulation," *New Journal of Physics*, vol. 15, no. May 2013, 2013.

[9] P. Elwenspoek and Dr.ir.R.J.Wiegerink, *Mechanical Microsensors*, 2018.

[10] H. Soemers, *Design principles for precision mechanisms*, 2017.

[11] W. C. Young and R. G. Budynas, *Roark ' s Formulas for Stress and Strain*.

[12] M. Elwenspoek, G. Krijnen, R. Wiegerink, and T. Lammerink, *Introduction to Mechanics and transducer science*. Enschede: University of Twente, 2011.

[13] IDS, "Process Document MEMS."

[14] Analog Devices, "Low Noise, Low Drift, Low Power, 3-Axis MEMS Accelerometers ADXL354/ADXL355," pp. 1–42, 2016.

[15] D. Alveringh, R. A. Brookhuis, R. J. Wiegerink, and G. J. Krijnen, "A large range multi-axis capacitive force/torque sensor realized in a single SOI wafer," *Proceedings of the IEEE International Conference on Micro Electro Mechanical Systems (MEMS)*, pp. 680–683, 2014.

APPENDIX A
OPTIMUM FINGER DISTANCE

To use the available area to its maximum all the dimensions are important. It is a complicated puzzle to make a decision between how much of the area can be use for sensing fingers, how much for support structure and how much should be left open. Longer fingers lead to a higher sensitivity but also can start sagging or bending if they become too long. Also for finding the optimum distance between the fingers there is a complete study performed which resulted in a mathematical approach for finding the optimum [15].

The minimum thickness for the fingers is $3.5\ \mu m$, preferably a safety measure is taken into account for this. Therefore $5\ \mu m$ is chosen as a safe thickness for the fingers. The same limitation holds for the minimum distance between structures, which should at least be $5\ \mu m$.

The distance between two parallel plates will be called d_0. Then there is the distance to the neighbouring parallel plate pair, which will be called d_1. Because of the orientation of the fingers and they way they interconnect to form combs the neighbouring finger will have a negative effect on the capacitance. Ideally this distance is as large as possible. The problem being that a large distance between the finger pairs does not efficiently use the available area.

Taking into account both the increase and decrease of capacitance when the distance moves an equation can be formed of which its derivative shows a maximum [15].

$$\frac{\partial}{\partial d_1}\frac{1}{d_0+d_1+2W_{finger}}\left(\frac{1}{d_0}-\frac{0}{d_1}\right)=0 \qquad (17)$$

W_{finger} is the width of the fingers which is $5\ \mu m$, now if we choose either d_0 or d_1 the equation is solvable. In this case d_0 is chosen to be $5\ \mu m$ which is as small as possible with a good safety margin. The resulting d_1 is $15\ \mu m$.

APPENDIX B
CAPACITANCE READOUT

As discussed the readout structure consists of two capacitors (C_1 & C_2), which are mirrored versions of each other. Both the structures consist of an amount of parallel plate capacitors (770 pairs each) but they also consist of parts that provide electrical and mechanical connections for the parallel plate capacitors to work. Every part that is electrically connected will create a capacitance. Some of these capacitances are desired, others are unwanted and are considered parasitic. This Appendix will give a detailed breakdown of all the capacitances and their influence.

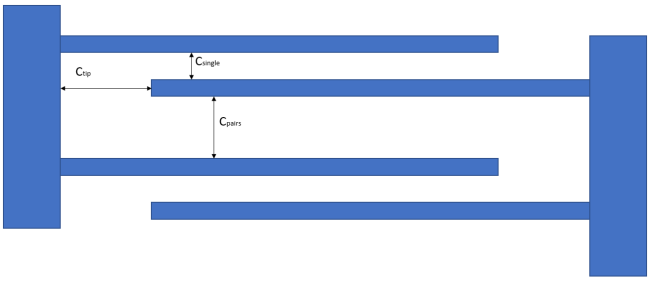

Fig. 37: Two pairs of parallel plate capacitors and the occurring capacitances in a horizontal orientation.

Figure 37 shows two parallel place capacitors. In this figure 3 capacitances are visible. C_{single} is the capacitance of a single parallel plate capacitor. This capacitance changes when the distance between the individual fingers changes, which is a result of a movement of the mass. The change in capacitance is given by:

$$C = \frac{\epsilon A}{x} \tag{18}$$

And the area is determined by the dimensions of the fingers as are visible in Table II. C_{pairs} is the capacitance between two parallel plate capacitors, this distance changes in the opposite direction as C_{single} but can be described with the same equation and dimensions. The difference is that the initial distance is 15 μm instead of 5 μm. The last capacitance is that of C_{tip} this is the capacitance between the finger connected to the mass to the structure that supports the sensing fingers. This capacitance is constant because despite of the movement of the fingers there is no change in distance or area in the direction of C_{tip}. The static values of the capacitances are given in Table VI.

TABLE VI: The different capacitances and their static values.

Capacitance	Value
C_{single}	1.04×10^{-14} F
C_{pairs}	3.47×10^{-15} F
C_{tip}	7.38×10^{-17} F

TABLE VII: All the different capacitances, calculated by their total area and distance between structures. Capacitances are divided by their vertical or horizontal orientation in the chip.

Vertical Parasitics	Area	Unit
Area Fingers	3850000	µm^2
Area Finger support	882400	µm^2
Area Horizontal support	334654,645	µm^2
Total Area	5067054,645	µm^2
Parasitic_static to mass	**2,24E-11**	**F**
Static structure to handle layer		
Area bondpads + connections	557400	µm^2
Area outer structure	296400	µm^2
stopper blocks	45000	µm^2
Total Area	898800	µm^2
Parasitic_static to handle	**1,55E-11**	**F**
Moveable part to handle layer (air)		
Area U-bends	252200	µm^2
Area springs	4340	µm^2
Total Area	256540	µm^2
Parasitic_moveable to handle (air)	**1,14E-12**	**F**
Moveable part to handle layer (SiO2)		
Area bondpads + connections	278700	µm^2
Area spring anchors	19600	µm^2
Total Area	298300	µm^2
Parasitic_moveable to handle (SiO2)	**5,15E-12**	**F**
Horizontal parasitics		
Finger tips		
Area finger tips	192500,00	µm^2
Parasitic_finger tips	**1,14E-13**	**F**
Mass to handle		
Circumference trench	6640000,00	µm^2
Parasitic_Mass to bulk	**6,53E-13**	**F**
Static structure to bulk		
Bondpads	113000	µm^2
Bondpad connections	135000	µm^2
Outer structure	240000	µm^2
Total Area	488000	µm^2
Parasitic_ structure to bulk (static)	**2,16E-13**	**F**
Moveable structure to bulk		
Bondpads (mass)	56500	µm^2
Bondpad connections (mass)	77650	µm^2
Total Area	134150	µm^2
Parasitic_structure to bulk (mass)	**5,94E-14**	**F**
Mass to bulk		
U-bends	133500	µm^2
Electrical connections	49500	µm^2
Total Area	183000	µm^2
Parasitic_mass to bulk	**8,10E-14**	**F**

Table VII shows different parts of the chip that cause capacitances at positions that are not the sensing fingers. In this table all the areas are for the entire accelerometer design. All the capacitances can be divided over the following three terms; C_p which are all the parasitic capacitances. A capacitance is considered parasitic if it is a capacitance that is not influenced by the desired direction of movement. The other two terms are C_1 & C_2 which are equal to each other and both consist of half of the readout structure.

APPENDIX C
MASK DESIGNS

Presented in the paper are two different accelerometer designs. First the initial design which has a readout structure in the device layer that is suspended above a mass which is located in the handle layer. The complete mask design is visible in Figure 38.

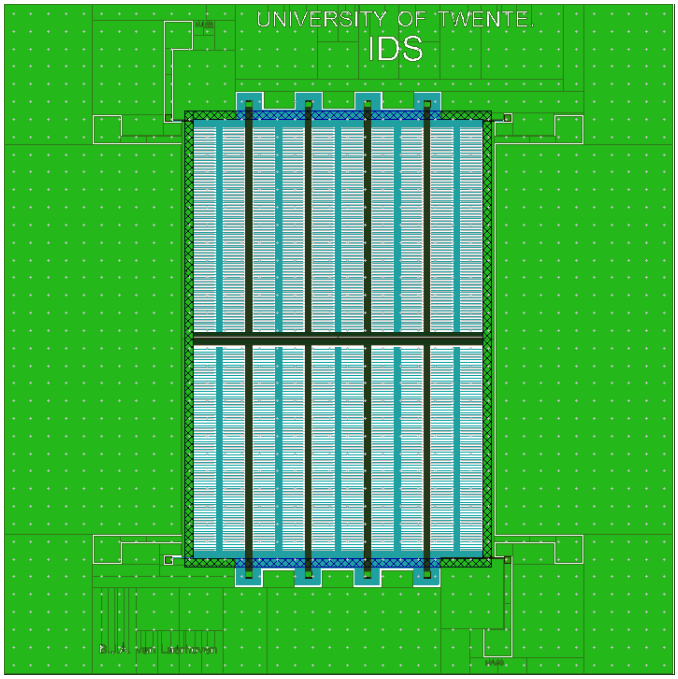

Fig. 38: Snapshot of Clewin5 which displays the mask design. (Dark) green indicates parts connected to the reference frame. Blue is connected to the mass and is free the move.

Figure 39 shows a zoomed in version on one of the capacitors. Visible in blue is the structure that is connected to the mass. Pink indicates the fingers that are connected to the reference frame which in this case is the freely hanging structure. Also visible are the four anchors on top from which the structure is supported. The blue material surrounding the anchors is connected to the mass but is necessary to create a good electrical connection for the output.

Now the second accelerometer design, which has a freely moving readout structure. The structure can no longer be connected to the anchors, so they are removed. Instead extra springs are added to suspend the readout structure, as is already discussed in the paper. Figure 40 shows the complete Clewin mask for the second accelerometer design.

Figure 41 shows a zoomed in version on one of the capacitors. Blue is still the material that is connected to the mass. Pink is the material that is part of the readout structure and will be brought to oscillation with the EMAM principle.

Figure 42 shows one of the actuator structures that is used for moving the readout structure. The pink material is fixed

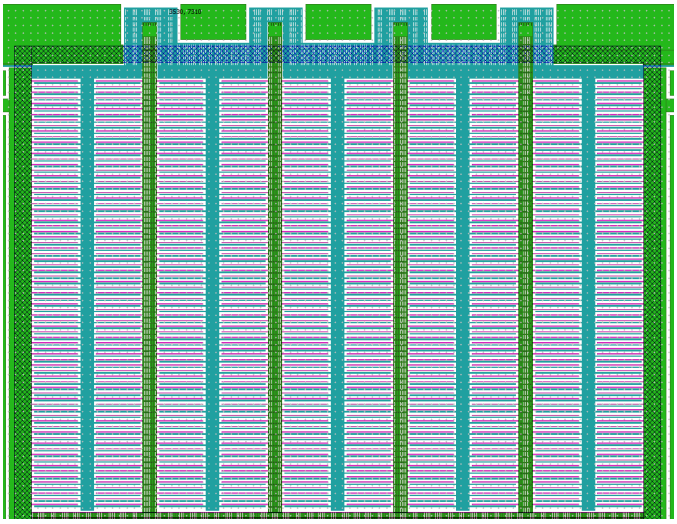

Fig. 39: Snapshot of Clewin5 which displays the mask design. Zooming in on one of the capacitor structures. Blue indicates the material connected to the mass.

to the readout structure. This connection is only mechanical because SiN isolation trenches are used to isolate the different electrical signals. Also visible are the low stiffness springs that are connected to all the combs.

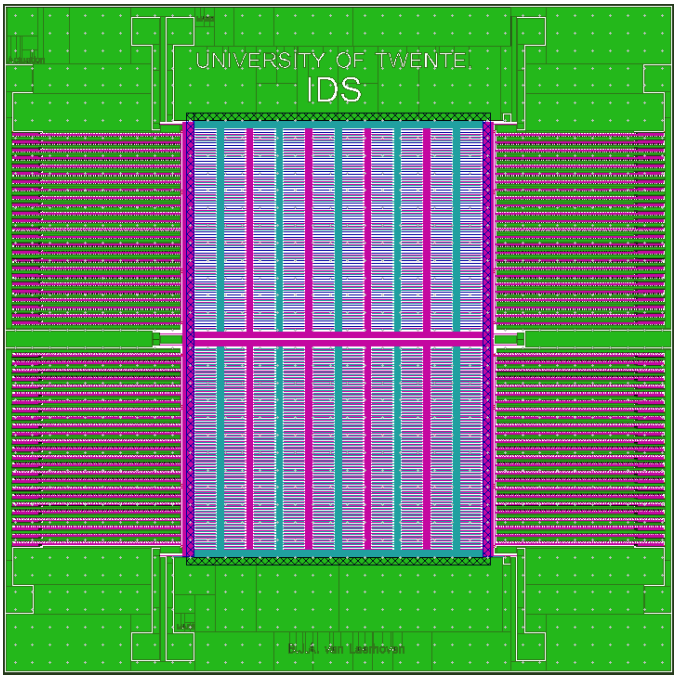

Fig. 40: Snapshot of Clewin5 showing the complete mask design of the chip with a moveable readout. Green indicates parts connected to the reference frame. Blue is connected to the mass and purple indicates the freely moving readout structure.

Fig. 41: Snapshot of Clewin5 which displays the mask design. Zooming in on one of the capacitor structures. Blue indicates the material connected to the mass. Pink is material that makes up the moveable readout structure.

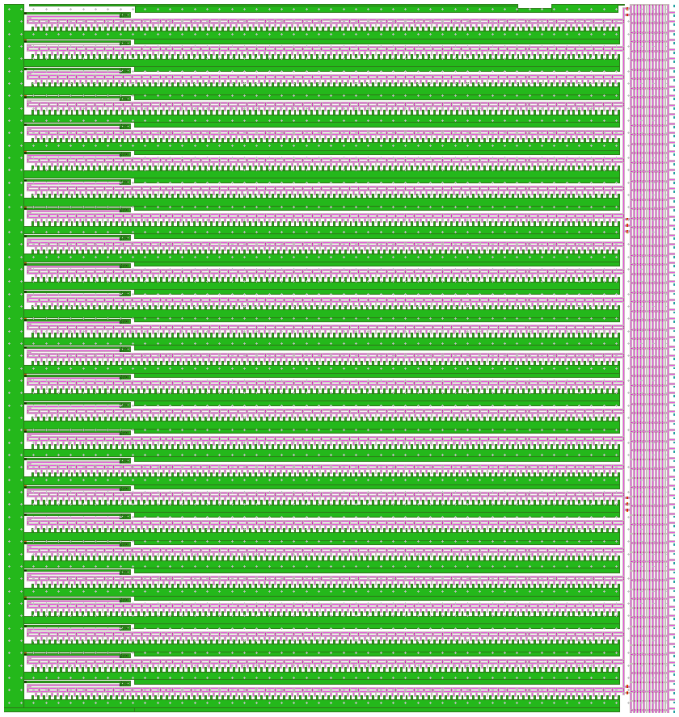

Fig. 42: Snapshot of Clewin5 which displays the mask design. Zooming in on one of the actuator structures. Pink is moveable, green is fixed material.

APPENDIX D
PCB DESIGN

This appendix gives additional information on the design of the PCBs that are used in the measurement setup. The PCBs are designed in AutoDesk EAGLE, and produced by Eurocircuits.
The paper shows and discusses the layout of one PCB, this PCB is designed for connecting several designs of the accelerometer microchips that were made available to test the measurement setup. A second PCB design is created for connecting the accelerometer of the two designs discussed in this paper. An important difference is that the proposed designs use a mass in the handle layer, therefore we need to make sure that there is room underneath the chip for the mass to freely move. This will be discussed in more detail.

The start of the PCB design was to use the building blocks that are already available within the research group. Throughout the years testing devices have been developed and perfected that work well for testing accelerometers. This involves a baseboard, a chipboard and several plug-in modules that can be connected to the baseboard. Together these parts form a pretty bulky and big setup. In the measurement setup this should all be mounted on top of the shaker. This would be very complicated to realise. A better method is to design a smaller PCB that only contains the necessary electronics and can easily be mounted on the shaker.

The design of the PCB starts by taking parts of the already existing measurement setup. The baseboard is the bridge between the chip and the amplyfing electronics. To prepare the signal a front-end chargeamp is present. This consists of a JFET and a feedback loop with the feedback capacitor and resistor, the schematic is visible in Figure 43. Connected to this baseboard is a charge amplifier module that further amplifies the signal. This module consists of operational amplifier and uses the value of the feedback capacitor to determine the gain. The module also contains the necessary electronics to power the amplifier and there is a demodulator to immediately demodulate the signal. This eliminates the use of a lock-in amplifier.

The demodulator is taken out of the design since an external lock-in amplifier will be used. The schematic of the operational amplifier is copied and combined with the schematic for the front-end chargeamp. The combination of the electronics leads to the schematic visible in Figure 44.

The microchip needs to fit somewhere on the PCB, therefore an area is designed where the chip will be located, surrounding this area bondpads are created to which wirebonds can be connected. The placement of these bondpads resembles the positions of the bondpads on the microchips. This keeps the wirebonds as short as possible and prevent wires from crossing or touching each other. The PCB for the accelerometer designs proposed in this paper there is an extra addition that the area underneath the mass of the

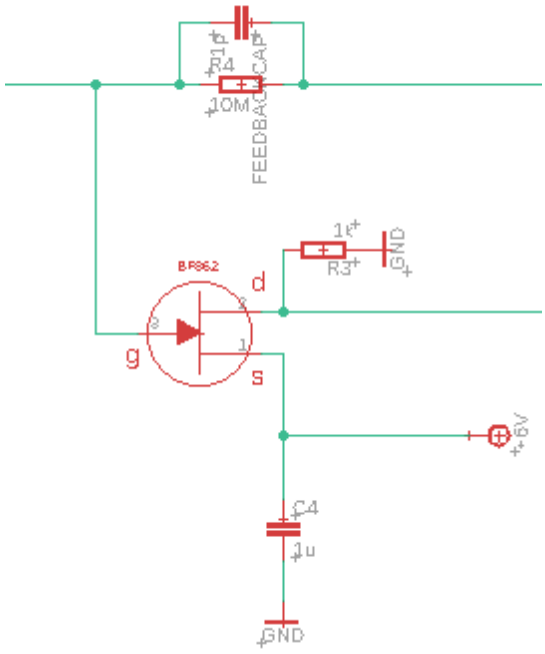

Fig. 43: Snapshot of EAGLE. Showing the electric schematic of the front-end chargeamp.

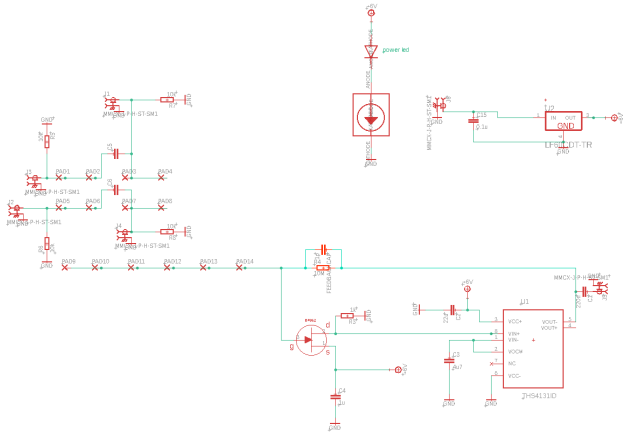

Fig. 44: Snapshot of EAGLE. Showing the complete electric schematic and all the parts.

microchip is made free and slightly lower as the copper layer surrounding it. The microchip needs to be outlined carefully to make sure that the mass is located above this open space so that it can freely move even if it drops slightly because of gravity.

To connect the PCB to the outside electronics MMCX coax connectors are used. The choice was made to use only surface mount components, this had the biggest impact on these coax connectors. For the general purpose PCB there are

6 connectors.

1) Readout input signal (V_{in})
2) Readout input signal ($-V_{in}$)
3) Output signal
4) Power supply
5) Feedback actuation signal (2x)

The general purpose PCB has connections that allow the actuator combs to be used for readout. By making two solder connections paths are created that connect these extra combs. When the connection is left open these combs will not be connected or they can be used for actuation by putting a signal on the actuation connectors.

The PCB designed specifically for the discussed designs has 8 coax connectors. Two connectors are added for signals for the actuation that causes the modulation of the readout structure. There is also an extra connection to combine these signals if they are operated with a single signal.

1) Readout input signal (V_{in})
2) Readout input signal ($-V_{in}$)
3) Output signal
4) Power supply
5) feedback actuation signal (2x)
6) Modulation actuation signal (2x)

Figures 45 & 46 show the EAGLE board designs of the PCBs. Figures 47 & 48 show the resulting PCB boards. Of both designs 10 PCBs were ordered. The parts that go on the PCBs were ordered elsewhere and the assembly was done personally. Included below is a parts list of all the components used on the PCB (Table VIII).

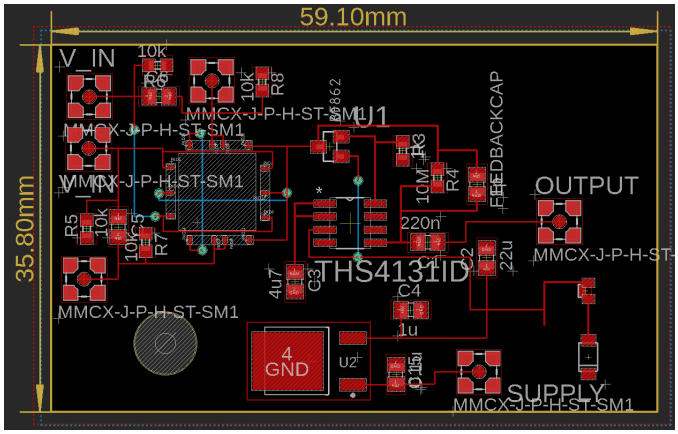

Fig. 45: Snapshot of EAGLE. Showing the PCB schematic for the general purpose design. Visible are all the components and traces.

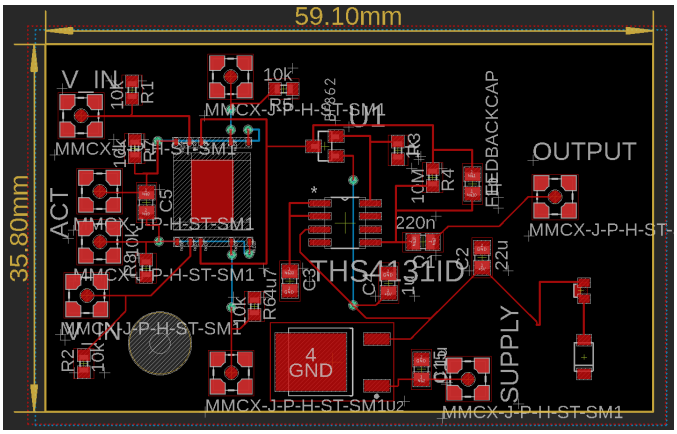

Fig. 46: Snapshot of EAGLE. Showing the PCB schematic for the accelerometer designs. Visible are all the components and traces.

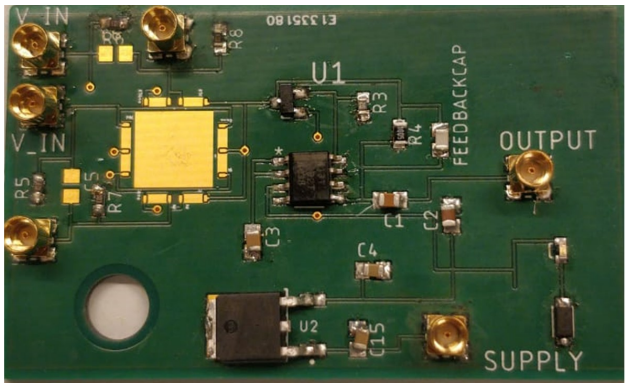

Fig. 47: Realisation of the general purpose PCB design.

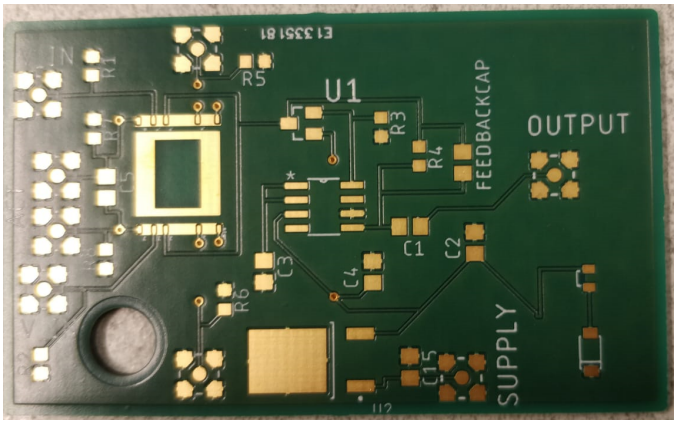

Fig. 48: Realisation of the own accelerometer design PCB. Components are not placed.

TABLE VIII: List of the parts used on the PCB designs, including their packages and values.

Part	Name	Package	Description / Value
U1	THS4131ID	-	Operational Amplifier
U2	LF60	-	Linear voltage regulator
T$2	BF862	-	JFET
U$11	KPA-1606QBC	-	LED
U$14	NS14502AT1G$_{CCR}$	-	LED driver
C1	Capacitor	C-EU0805	220n
C2	Capacitor	C-EU0805	22u
C3	Capacitor	C-EU0805	47u
C4	Capacitor	C-EU0805	1u
C15	Capacitor	C-EU0805	0.1u
FEEDBACKCAP	1p	C-EU0805	1p
J1-J8	MMCX-J-P-H-ST-SM1	-	COAX connectors
R3	Resistor	R-EU0603	1K
R4	Resistor	R-EU0603	10M
R5 - R8	Resistor	R-EU0603	10K

APPENDIX E
MEASUREMENT SETUP

The measurement setup is discussed in the paper. This section provides more details on the equipment that is used.

List of equipment used:

- HP/Agilent 33120A Function Generator (2x)
- Power supply (2x)
- Agilent DSO-X 3024A Oscilloscope
- Stanford Research Systems SR830 Lock-In Amplifier
- Shaker
- PM 5175 Philips Amplifier (shaker)
- Coax cables

The measurement setup starts with the PCB, a microchip is connected to the PCB using conducting tape, after that wirebonds are created between the bondpads of the microchip and the PCB. The PCB is mounted on the shaker.

The PCB is powered by one of the power supplies, the linear voltage regulator on the PCB works best for an input of 7.5 V.

The shaker is powered with an additional amplifier, the amplifier enhances a signal that is created by the oscilloscope. On the oscilloscope the desired frequency and amplitude can be selected which becomes the input for the shaker.

The oscilloscope has four inputs, one of the inputs is used for the reference sensor, another input is used for the output of the lock-in amplifier. The other two inputs can be used for debugging or checking if the system is operating properly.

The carrier signal is created with the two function generators, both function generators are set to the same frequency and amplitude, one function generator is set to a delay of half a cycle creating a $180°$ phase shift. The function generators are linked on the backside to time the triggers, this creates a master slave construction. When the 'master' function generator is triggered the 'slave' will automatically follow. In this way the second signal is always a perfect inverse of the first signal.

The output of the PCB first goes to the input of the lock-in amplifier. Connected to the lock-in amplifier is also one of the output signals of the function generator, this syncs the lock-in frequency. The lock-in amplifier has settings for the time constant and sensitivity, these need to be tuned to get a satisfactory output. This is dependent on the input frequency of the shaker and the performance of the accelerometer. The output of the lock-in amplifier is connected to the input of the oscilloscope to visualise the result.

Lastly the second power supply is used to power the reference sensor. The sensor performs best for an input voltage of 3.3 V DC.

APPENDIX F
IMPORTANT PARAMETERS

TABLE IX: Important parameters that are imported in the matlab code for the initial design.

Mass calculation	Value	Unit
Handle layer		
Length	5000.00	μm
Width	3300.00	μm
Height	380.00	μm
Weight	1.46E-05	Kg
Device layer		
Height	25.00	μm
Area comb structure	355274.50	μm^2
#comb structures	10.00	
Area electrical connections	413000.00	μm^2
Area U-bend	40975.00	μm^2
# U-bends	8.00	
Area U-bend connect	25800.00	μm^2
# U-bend connects	6.00	
Total area	4448345.00	μm^2
Weight	2.59E-07	Kg
Total weight	1.49E-05	Kg
Spring dimensions	Value	Unit
Length	250	μm
Width	7	μm
Height	25	μm
# springs	4	
Spring constant	373.184	N/m
Finger dimensions	Value	Unit
Length	250.00	μm
Width	5.00	μm
Height	25.00	μm
Overlap	235.00	μm
# parallel plates	1540.00	
Plate gap	5.00	μm
Capacitor gap	15.00	μm
Capacitances	Value	Unit
Parallel plate (single)	1.04E-14	F
Total capacitance	4.40E-11	F
Cp	6.37E-12	F
Parasitics		
Parasitic_between pairs	3.47E-15	F
Vertical		
Parasitic_static to mass	2.24E-11	F
Parasitic_static to handle	1.55E-11	F
Parasitic_moveable to handle (air)	1.14E-12	F
Parasitic_moveable to handle (SiO2)	5.15E-12	F
Parasitic_Mass to bulk	6.53E-13	F
Horizontal		
Parasitic_ structure to bulk (static)	2.16E-13	F
Parasitic_structure to bulk (mass)	5.94E-14	F
Parasitic_mass to bulk	8.10E-14	F

TABLE X: Important parameters that are imported in the matlab code for the moveable design.

Mass calculation	Value	Unit
Handle layer		
Length	5000.00	μm
Width	3300.00	μm
Height	407.00	μm
Weight	1.56E-05	Kg
Device layer		
Height	25.00	μm
Area comb structure	355687.50	μm^2
#comb structures	10.00	
Area electrical connections	523768.00	μm^2
Total area	4080643.00	μm^2
Weight	2.38E-07	Kg
Total weight	1.59E-05	Kg
Actuation calculation	Value	Unit
Height	25	μm
Area actuator	755975	μm^2
#actuators	4	
Area outer structure	746380	μm^2
Area sense combs	192500	μm^2
# sense combs	10	
Area sense comb structure	1122350	μm^2
Total area	6817630	μm^2
Total weight	3.97E-07	Kg
Spring constants	Value	Unit
Mass	373.18	N/m
Actuation	910.42	N/m
Resonance frequency	Value	Unit
Mass	771.59	Hz
Actuation	10779.17	Hz
Finger dimensions	Value	Unit
Length	250.00	μm
Width	5.00	μm
Height	25.00	μm
Overlap	235.00	μm
# parallel plates	1540.00	
Plate gap	5.00	μm
Capacitor gap	15.00	μm
Capacitances	Value	Unit
Parallel plate (single)	1.04E-14	F
Total capacitance	4.40E-11	F
Cp	6.64E+06	F
Parasitics		
Parasitic_between pairs	0.00E+00	F
Vertical		
Parasitic_static to mass	0.00E+00	F
Parasitic_static to handle	0.00E+00	F
Parasitic_moveable to handle (air)	0.00E+00	F
Parasitic_moveable to handle (SiO2)	6.64E+06	F
Parasitic_Mass to bulk	0.00E+00	F
Horizontal		
Parasitic_ structure to bulk (static)	0.00E+00	F
Parasitic_structure to bulk (mass)	0.00E+00	F
Parasitic_mass to bulk	0.00E+00	F

APPENDIX G
SIMULATIONS

This section shows a more detailed overview of how the simulations are built-up. A screenshot of all the subsystems will be given.

Figure 49 shows the all the building blocks of the total simulation. Also visible are the connections to the spectrum analyser and which information goes to the matlab code for possible further processing.

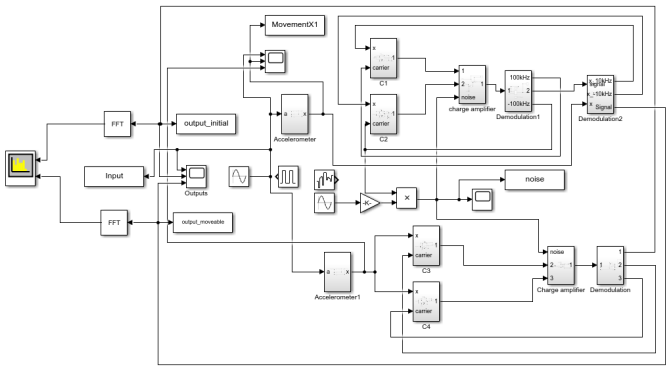

Fig. 49: Screenshot of Simulink. Showing all the building blocks of the simulation, how they are connected and which outputs go to matlab.

Figure 50 shows the first subsystem, which converts an acceleration to a movement of the mass. This simulates the mass-spring-damper equation. Visible are 3 gain blocks, which hold the parameters for mass (M), spring constant (K) and damping (D).

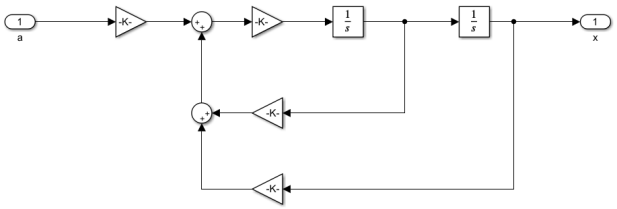

Fig. 50: Screenshot of Simulink. Showing the simulated spring-mass-damper system.

Figure 51 shows the subsystem of one of the capacitors. Equations 14 is simulated in this block. There are also some connections connected to a scope used for debugging. The eventual capacitance is multiplied with a gain which is set to the amount of finger pairs. Afterwards the carrier signal is added.

Figure 52 first shows a sum block where the signals C1 and C2 are combined. Visible is that there is a product block to introduce noise to the signal of C2. After that the gain block has a gain of $1/C_f$.

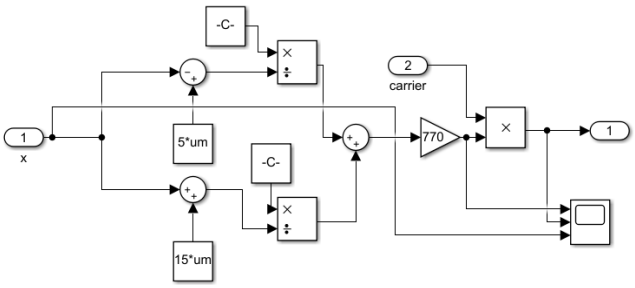

Fig. 51: Screenshot of Simulink. Showing the simulated equations that calculate the varying capacitance

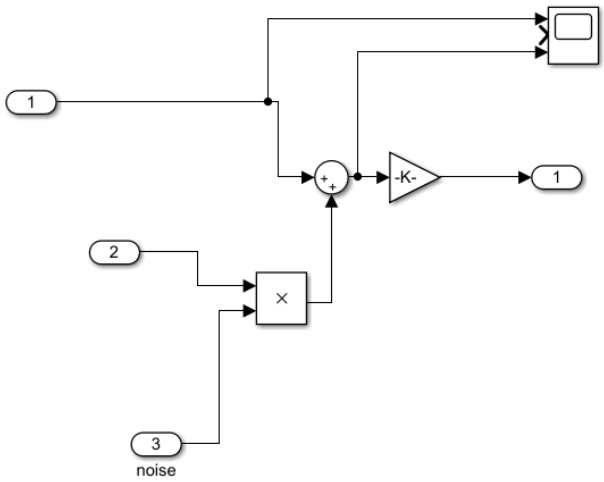

Fig. 52: Screenshot of Simulink. Showing the functioning of the charge amplifier and the combination of the signals C1 and C2.

Figure 53 shows the subsystem that holds the building blocks for the demodulation of the carrier signal. We see the generation of the two sine signals with a $180°$ phase shift. And how the signals enter the demodulation building block.

Figure 54 shows the second demodulation step. Here the carrier signal is visible that is used for generating the 10 kHz modulation that simulates the EMAM principle.

Figure 55 shows what happens within all the demodulation blocks. The carrier signal is multiplied again after which a 8th order Chebychev low-pass filter is used.

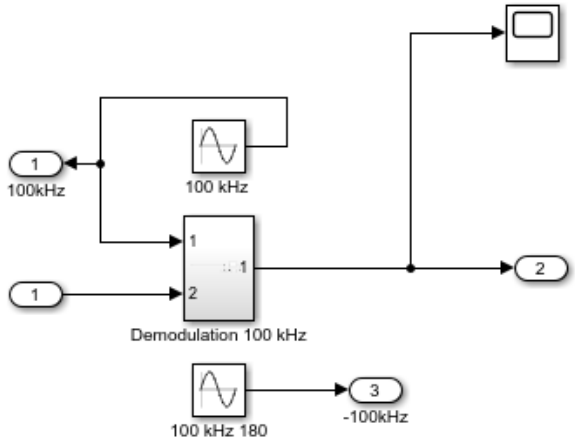

Fig. 53: Screenshot of Simulink. Showing the first demodulation for the 100 kHz carrier.

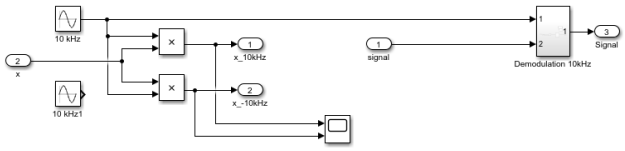

Fig. 54: Screenshot of Simulink. Showing the second demodulation for the 10 kHz modulation.

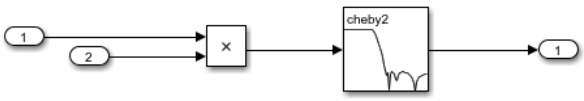

Fig. 55: Screenshot of Simulink. Showing the design of the low-pass filter.

APPENDIX H
MATLAB CODE

```
clear all;
close all;

opts = detectImportOptions('Numbers.xlsx');
opts.Sheet = 'Moveable readout';
Excel = readtable('Numbers.xlsx',opts);

results = struct;
constant = struct;
Spring = struct;
%% Constants
um = 10^-6; %Conversion to micrometer
constant.E0 = 8.854*10^-12; % vacuum permittivity F/m
constant.Er = 3.9; %permittivity Si02
constant.E = 170*10^9; %Young's modulus in Pa
constant.density_S = 2.3290*10^3; %kg/m^3 ~density Silicon
constant.Cf = 1e-12;


%% Springs
K_y = Excel{29,2};

K_act = Excel{30,2};

%% Proof masses
Mass.M1 = Excel{14,2};
Mass.M2 = Excel{26,2};

K_res = Mass.M2*(1*10^4*2*pi)^2; %Spring constant at resonance frequency of 10 kHz
%% Resonance frequency and quality factor
Q = 10; %Quality factor
Om_res = sqrt(K_y/Mass.M1); %Resonance frequency of Proof Mass 1
B= (Om_res*Mass.M1)/Q;
results.freq = (1/(2*pi))*Om_res; % Resonance frequency in Hz


Res_frequency2 = (1/(2*pi))*sqrt(K_act/(Mass.M2/2)); % Resonance frequency of Proof mass 2, used for actuation
B2 = (sqrt(K_act/Mass.M2))/Q;
Q_calc = (sqrt(K_act/Mass.M2))/B;

%% Simulink
%filter
Wn = 100/100000;
[cheb1,cheb2] = cheby2(2,40,Wn);
[z,p,k,] = cheby2(9,40,Wn);

%damping
D = (Om_res*Mass.M1)/Q;

%model
sim('Accelerometer_model_1309')


figure(1)
plot(tout,MovementX1*10^6)
xlabel('Time [sec]')
ylabel('Movement of Mass [um]')
title('Movement at 1G acceleration input')


%%
figure(2)
hold on
plot(tout,output_initial)
plot(tout,output_moveable)
xlabel('Time [sec]')
ylabel('Output voltage [V]')
title('Voltage output against time for 1 G acceleration input')
legend('initial design', 'moveable readout')

fs = 2000000; %2 MHz
T = 1/fs;
L = length(tout);
t = (0:L-1)*T;
n = length(output_initial);
%analyse1 = fft(output_initial);
analyse1 = fft(output_moveable);
P2 = abs(analyse1/L).^2/n;
P1 = P2(1:L/2+1);
P1(2:end-1) = 2*P1(2:end-1);

f = fs*(0:(L/2))/L;
f2 = (0:n-1)*(fs/n);
power = abs(analyse1).^2/n;
y0 = fftshift(analyse1);          % shift y values
f0 = (-n/2:n/2-1)*(fs/n); % 0-centered frequency range
power0 = abs(y0).^2/n;     % 0-centered power

figure(8)
plot(f,P1)
figure(9)
plot(f0,power0)

```

```
%% Test
test = results.freq/(900/5);

%% Finger dimensions
A_sense = Excel{40,2}*Excel{39,2};
Finger_amount = Excel{41,2};


%% readout combs
gap_sense = 5*um; %Gap between fingers creating a parallel plate capacitor
gap_notsense = 15*um; % Gap to the next finger pair, optimum determined

%Pull-in voltage for the readout combs, driving voltage must be below the
%pull-in
Pull_in = sqrt((8*K_y*Excel{43,2}^3)/(27*constant.E0*Excel{41,2}*A_sense));
%V0 = 1:1:Pull_in; %Initial voltage V

%Maximum displacement before pull-in occurs
x_eq = 2/3*gap_sense;
results.max_allowed_defl = gap_sense - x_eq;

%a = 9.81;% 1G = 9.81 m/s^2
%movement_y = (Mass.M/results.K_y)*a; %in meters
%movement_z = (Mass.M/K_z)*a; %in meters
%x = 0:1*10^-8:movement_y;

%% Actuation combs
%Dimensions and calculations for the actuation combs
overlap = 3*um;
A_act = overlap*Excel{39,2};
gap_act = 4*um;
fingers = 25*210*2;
%Pull-in determines the maximum voltage that can be used for driving the
%actuators
Pull_in_act = sqrt((8*K_act*gap_sense^3)/(27*constant.E0*fingers*A_act));
voltage = 30;

%Resulting movement as a result of amount of fingers, spring constant and
%driving voltage
%Movement = (1/um)*(fingers*((constant.E0*Spring.height)/(K_act*gap_act))*voltage^2); %movement in um
Range = [0:1:7];
a = 9.81;% 1G = 9.81 m/s^2
movement_y = (Mass.M1/K_y)*Range*a*(1/um); %in micrometers
%% Output capacitance
x = -movement_y(1,8):0.1:movement_y(1,8); %in micrometers

%grid + finger tips capacitance
Capacitance.C0 = (Excel{55,2}/2) + um^2*Excel{41,2}*(constant.E0*Excel{38,2}*Excel{39,2})/Excel{44,2};

Capacitance.finger1 = um*((constant.E0*Excel{39,2}*Excel{40,2})./(Excel{43,2}-x));
Capacitance.notfinger1 = um*((constant.E0*Excel{39,2}*Excel{40,2})./(Excel{44,2}+x));
Capacitance.C1 = (Excel{41,2}/2)*(Capacitance.finger1+Capacitance.notfinger1)+Capacitance.C0;

Capacitance.finger2 = um*((constant.E0*Excel{39,2}*Excel{40,2})./(Excel{43,2}+x));
Capacitance.notfinger2 = um*((constant.E0*Excel{39,2}*Excel{40,2})./(Excel{44,2}-x));
Capacitance.C2 = (Excel{41,2}/2)*(Capacitance.finger2+Capacitance.notfinger2)+Capacitance.C0;

%sensitivity for 1 capacitor, total is 2x
results.sens = 1e12*(Capacitance.C1/Excel{43,2}); % in pF/um

figure(2)
hold on
plot(x,(Capacitance.C1)*1e12)
plot(x,(Capacitance.C2)*1e12)
title('Capacitance change with movement')
xlabel('movement [um]')
ylabel('Capacitance [pF]')
legend('C1','C2')

%% Voltage calculation
Vin = 10;
%V_in = ans.V_in;
Vout = ((Capacitance.C1 - Capacitance.C2)/constant.Cf).*Vin;
%sens = (1/2)*1e12*(Excel{40,2}/Excel{35,2}); % in pF/um
sens_V = 2.9*Vin;
sens_C = 2.9;
%b = Excel{40,2}*1e12;
b = 0;
y_V = sens_V*x + b;
y_C = sens_C*x;
```

```
Accel = (um/9.81)*(K_y*x)/Mass.M1;


figure(3)
hold on
plot(x,(Capacitance.C1-Capacitance.C2)*1e12)
plot(x,y_C)
legend('model','fitted line')
xlabel('movement [um]')
ylabel('Capacitance [pF]')


figure(4)
hold on
plot(Accel,Vout)
plot(Accel,y_V)
legend('model','fitted line')
xlabel('Acceleration [g]')
ylabel('Output voltage [V]')

%% 1 G region
Region.Accel = Accel(26:34);
Region.Vout = Vout(26:34);
Region.y_V = y_V(26:34);

figure(5)
hold on
plot(Region.Accel,Region.Vout)
plot(Region.Accel,Region.y_V)
legend('model','fitted line')
xlabel('Acceleration [g]')
ylabel('Output voltage [V]')

figure(6)
title('Simulation results for a 1G acceleration input')
subplot(3,1,1)
plot(tout,Input)
title('Input')
xlabel('Time [sec]')
ylabel('Output [V]')
subplot(3,1,2)
plot(tout,output_initial)
title('Initial design')
xlabel('Time [sec]')
ylabel('Output [V]')
subplot(3,1,3)
plot(tout,output_moveable)
title('moveable readout')
xlabel('Time [sec]')
ylabel('Output [V]')

figure(7)
plot(tout,noise*10^-11)
title('Simulated random signal that is applied to the acceleromters')
xlabel('Time [sec]')
ylabel('Capacitance[F]')
%%
[sos] = zp2sos(z,p,k);
h = fvtool(sos)

%% Parasitics
%All the other capacitances that occur in the chip which cause parasitic
%effects

%static perforated parts (capacitance to mass, oxygen)
Area.p1 = 8*102125*(um^2); %amount and area of perforated support beams (vertical)
Area.p2 = 1600*Excel{4,2}*Finger.Length; % amount and area of the static fingers
Area.p3 = 667755*(um^2); % area of perforated support beams (horizontal)
Parasitic.static = constant.E0*(Area.p1 + Area.p2 + Area.p3)/(2*um);

%connecting parts outer structures fixing the static perforated parts
%including bondpads
%(capacitance to handle layer, Sio2)
Area.p4 = 6*300*300*um^2;
Area.p5 = 6*750*70*um^2;
Parasitic.bondpad = (constant.E0*constant.Er)*(Area.p4+Area.p5)/(2*um);
Area.p6 = 4*2375*75*um^2;
Parasitic.connect = (constant.E0*constant.Er)*(Area.p6)/(2*um);

%parasitic at the finger tips
Area.p7 = Finger.amount*Finger.height*Finger.thick;
Parasitic.finger_tips = constant.E0*(Area.p7)/(2*um);

%parasitic of mass to ground
Area.p8 = 2*(8000*380)*um^2;
Parasitic.mass_ground = constant.E0*(Area.p8)/(90*um);

%F_ext = ((fin_act*E0*F_h)/gap_comb)*V0.^2;
%deflection = ((fin_act*E0*F_h)/(K_y*gap_comb))*V0.^2;

%% Ideal ratio gap_sense to gap_notsense
% the gap_sense is the distance between to sensing fingers
```

```
% the gap_notsense is the distance to the next finger pair, causing an
% unwanted capacitance
syms d1
d0 = gap_sense*10^6;
W = Finger.thick*10^6;
eqn(d0) = (-d1.^2+2.*d1.*d0+d0.^2+2.*W.*d0)./(d1.^2.*d0.*(d1+d0+2.*W).^2) == 0;
optimum_gap_notsense = solve(eqn,d1,'Real',true);
```